

**Formation,  
composition, and  
phase of  $\alpha$ -cedrene  
SOA**

Y. Zhao et al.

This discussion paper is/has been under review for the journal Atmospheric Chemistry and Physics (ACP). Please refer to the corresponding final paper in ACP if available.

# Phase, composition and growth mechanism for secondary organic aerosol from the ozonolysis of $\alpha$ -cedrene

Y. Zhao, L. M. Wingen, V. Perraud, and B. J. Finlayson-Pitts

Department of Chemistry, University of California, Irvine, CA 92697, USA

Received: 18 November 2015 – Accepted: 24 November 2015

– Published: 14 December 2015

Correspondence to: B. J. Finlayson-Pitts (bjfinlay@uci.edu)

Published by Copernicus Publications on behalf of the European Geosciences Union.

Title Page

Abstract

Introduction

Conclusions

References

Tables

Figures



Back

Close

Full Screen / Esc

Printer-friendly Version

Interactive Discussion



## Abstract

Sesquiterpenes are an important class of biogenic volatile organic compounds (BVOCs) and have a high secondary organic aerosol (SOA) forming potential. However, SOA formation from sesquiterpene oxidation has received less attention compared to other BVOCs such as monoterpenes, and the underlying mechanisms remain poorly understood. In this work, we present a comprehensive experimental investigation of the ozonolysis of  $\alpha$ -cedrene both in a glass flow reactor (27–44 s reaction times) and in static Teflon chambers (30–60 min reaction times). The SOA was collected by impaction or filters, followed by analysis using attenuated total reflectance-Fourier transform infrared spectroscopy (ATR-FTIR) and electrospray ionization mass spectrometry (ESI-MS), or measured on line using direct analysis in real time (DART-MS) and aerosol mass spectrometry (AMS). The slow evaporation of 2-ethylhexyl nitrate that was incorporated into the SOA during its formation and growth gives an estimated diffusion coefficient of  $3 \times 10^{-15} \text{ cm}^2 \text{ s}^{-1}$  and shows that SOA is a highly viscous semi-solid. Possible structures of four newly observed low molecular weight ( $\text{MW} \leq 300 \text{ Da}$ ) reaction products with higher oxygen content than those previously reported were identified. High molecular weight (HMW) products formed in the early stages of the oxidation have structures consistent with aldol condensation products, peroxyhemiacetals, and esters. The size-dependent distributions of HMW products in the SOA, as well as the effects of stabilized Criegee intermediate (SCI) scavengers on HMW products and particle formation, confirm that HMW products and reactions of Criegee intermediates play a crucial role in early stages of particle formation. Our studies provide new insights into mechanisms of SOA formation and growth in  $\alpha$ -cedrene ozonolysis and the important role of sesquiterpenes in new particle formation as suggested by field measurements.

### Formation, composition, and phase of $\alpha$ -cedrene SOA

Y. Zhao et al.

Title Page

Abstract

Introduction

Conclusions

References

Tables

Figures



Back

Close

Full Screen / Esc

Printer-friendly Version

Interactive Discussion



## 1 Introduction

Organic aerosol is ubiquitous in the atmosphere and has an important influence on air quality (Finlayson-Pitts and Pitts, 2000; Seinfeld and Pandis, 2006; R. Y. Zhang et al., 2015), climate (Kanakidou et al., 2005; IPCC, 2013), and human health (Mauderly and Chow, 2008; Shiraiwa et al., 2012). Secondary organic aerosol (SOA) formed from the oxidation of volatile organic compounds (VOCs) contributes a substantial fraction (up to 90 %) of organic aerosol (Zhang et al., 2007). Biogenic VOCs (BVOCs) such as isoprene (C<sub>5</sub>H<sub>8</sub>), monoterpenes (C<sub>10</sub>H<sub>16</sub>), and sesquiterpenes (C<sub>15</sub>H<sub>24</sub>) account for ~ 90 % of global VOC emissions (Guenther et al., 1995; Goldstein and Galbally, 2007) and are the dominant contributors to global SOA formation upon reaction with oxidants that are mainly anthropogenically derived (Kanakidou et al., 2005; Hallquist et al., 2009).

Sesquiterpenes are an important class of BVOCs, with emissions being estimated as 9–29 % of those of monoterpenes (Helmig et al., 2007; Sakulyanontvittaya et al., 2008a). A variety of sesquiterpenes have been detected in the atmosphere, including  $\beta$ -caryophyllene,  $\alpha$ -humulene, longifolene,  $\alpha$ -farnesene, and  $\alpha$ -cedrene (Helmig et al., 2007; Sakulyanontvittaya et al., 2008a; Duhl et al., 2008; Bouvier-Brown et al., 2009). Sesquiterpenes have a high SOA forming potential because of their large molecular sizes and, for many of them, the endocyclic double bond structure which favors the formation of low-volatility oxidation products. The results of laboratory chamber studies show high aerosol mass yields (defined as the mass of organic aerosol formed per mass of precursor VOC reacted) from sesquiterpene oxidation (Hoffmann et al., 1997; Lee et al., 2006; Ng et al., 2006; Winterhalter et al., 2009; Chen et al., 2012; Jaoui et al., 2013; Yao et al., 2014; Tasoglou and Pandis, 2015). For example, an average 53 % aerosol mass yield was reported for ozonolysis and 55 % for photooxidation (Jaoui et al., 2013). Field and model studies have shown that sesquiterpene SOA comprises a significant fraction (6–32 %) of ambient organic aerosol (Sakulyanontvittaya et al., 2008b; Hu et al., 2008; Bouvier-Brown et al., 2009; Ding et al., 2014; Ying et al., 2015),

### Formation, composition, and phase of $\alpha$ -cedrene SOA

Y. Zhao et al.

Title Page

Abstract

Introduction

Conclusions

References

Tables

Figures



Back

Close

Full Screen / Esc

Printer-friendly Version

Interactive Discussion



with its contribution comparable to that of monoterpene SOA in some environments (Hu et al., 2008; Ding et al., 2014).

Although sesquiterpene oxidation contributes substantially to SOA, the underlying mechanisms of SOA formation and growth are not well understood. Previous studies of sesquiterpene oxidation have mainly focused on aerosol mass yields, the identities and formation mechanisms of first-, second-, and higher-generation low molecular weight (LMW) oxidation products, and their contributions to the formation of SOA (Hoffmann et al., 1997; Jaoui et al., 2004, 2013; Lee et al., 2006; Ng et al., 2006; Kanawati et al., 2008; Reinnig et al., 2009; Winterhalter et al., 2009; Li et al., 2011; Chan et al., 2011; Chen et al., 2012; Alfarra et al., 2012; Yao et al., 2014). A few studies have suggested that sesquiterpenes play an important role in new particle formation. For instance, field observations show that in new particle formation events, sesquiterpene oxidation products significantly contribute to initial nucleation and growth (Boy et al., 2008; Bonn et al., 2008). In addition, Bonn and Moortgat (2003) suggested that the formation of oligomers was potentially important for nucleation. Lastly, laboratory studies of the ozonolysis of  $\beta$ -caryophyllene and  $\alpha$ -cedrene have reported a negative influence on particle nucleation of species that can scavenge stabilized Criegee intermediate (SCI), supporting a key role for sesquiterpene SCI in forming new particles (Bonn and Moortgat, 2003; Yao et al., 2014).

$\alpha$ -Cedrene (Fig. 1) is found in air (Duhl et al., 2008) and reacts rapidly with O<sub>3</sub> (Richters et al., 2015). Previous studies of  $\alpha$ -cedrene oxidation identified a number of products with molecular masses below 300 Da in both the gas and particle phases, and proposed reaction mechanisms based on known ozone chemistry (Jaoui et al., 2004, 2013; Reinnig et al., 2009; Yao et al., 2014). Preliminary results from our lab (Zhao et al., 2015) subsequently identified higher molecular weight products in the  $\alpha$ -cedrene ozonolysis for the first time, and the SOA composition suggested that the major mechanisms for particle formation are likely different than that for the small alkenes (Sadezky et al., 2008; Zhao et al., 2015).

## Formation, composition, and phase of $\alpha$ -cedrene SOA

Y. Zhao et al.

Title Page

Abstract

Introduction

Conclusions

References

Tables

Figures



Back

Close

Full Screen / Esc

Printer-friendly Version

Interactive Discussion



**Formation,  
composition, and  
phase of  $\alpha$ -cedrene  
SOA**

Y. Zhao et al.

Title Page

Abstract

Introduction

Conclusions

References

Tables

Figures

◀

▶

◀

▶

Back

Close

Full Screen / Esc

Printer-friendly Version

Interactive Discussion

There have been very few measurements of the phase state of sesquiterpene SOA. The phase state of SOA has an important influence on a number of physical and chemical processes of aerosols, such as formation and growth (Koop et al., 2011; Perraud et al., 2012; Shiraiwa and Seinfeld, 2012; Renbaum-Wolff et al., 2013), chemical aging (Renbaum and Smith, 2009; Shiraiwa et al., 2011; Lignell et al., 2014; Chan et al., 2014; Slade and Knopf, 2014), and water uptake (Mikhailov et al., 2009; Koop et al., 2011; Bones et al., 2012; Hodas et al., 2015; Pajunoja et al., 2015), and thus affects their environmental and climate impacts. There is ample evidence that in many cases, SOA may not be a low-viscosity liquid but rather a highly viscous semi-solid (Virtanen et al., 2010; Cappa and Wilson, 2011; Koop et al., 2011; Vaden et al., 2011; Saukko et al., 2012; Perraud et al., 2012; Abramson et al., 2013; Renbaum-Wolff et al., 2013; Kidd et al., 2014a, b; Bateman et al., 2015). Recently, Saukko et al. (2012) and Pajunoja et al. (2015) examined the phase state of SOA particles formed from OH and O<sub>3</sub> oxidation of longifolene based on particle bounce measurements and found that longifolene SOA is solid or semi-solid over a wide range of relative humidities. To better understand the phase state of sesquiterpene SOA and its implications for various atmospheric processes, more particle phase state measurements are needed.

In the present study, we report the results of a more comprehensive experimental investigation of ozonolysis of  $\alpha$ -cedrene. The phase state and mechanisms of growth of SOA are examined by probing the evaporation of a tracer molecule, 2-ethylhexyl nitrate (2-EHN), incorporated into the SOA during ozonolysis. The structures and formation mechanisms of high molecular weight (HMW) products, as well as their roles in particle formation and growth, are elucidated in light of their fragmentation mass spectra, accurate mass data, size-dependent SOA composition, and the effects of water vapor and SCI scavenger. The identity and formation mechanisms of some newly observed LMW (MW < 300 Da) oxidation products are also explored.

## 2 Experimental

Experiments on  $\alpha$ -cedrene ozonolysis were carried out both in a glass flow reactor and in static Teflon chambers in the absence and presence of water vapor or SCI scavengers at  $295 \pm 1$  K. No seed particles or OH scavengers were used in any of these experiments. Table 1 and Fig. S1 in the Supplement summarize the conditions and particle characteristics for various types of flow reactor and chamber experiments.

### 2.1 Flow reactor experiments

The flow reactor (4.6 cm i.d. and 85 cm long) used in this study has been described in detail previously (Zhao et al., 2015).  $\alpha$ -Cedrene was added to the flow reactor by injecting the pure liquid (Sigma-Aldrich and Extrasynthese, > 98%) into a flow of  $1.76$ – $2.96$  L min<sup>-1</sup> of clean, dry air (Praxair, ultra zero air) using an automated syringe pump (Pump Systems Inc., model NE-1000). Ozone was generated by passing a flow of O<sub>2</sub> (Praxair, Ultra High Purity, 99.993%) at  $0.24$  L min<sup>-1</sup> through a pen-ray mercury lamp (model 11SC-2), and subsequently added to the flow reactor downstream of the  $\alpha$ -cedrene inlet. The O<sub>3</sub> concentration, determined using a UV-VIS spectrometer (Ocean Optics, HR4000), was adjusted by changing the UV exposure of the O<sub>2</sub> via a movable metal cover surrounding the lamp. The total flow rate in the reactor was  $2.0$ ,  $2.9$ , or  $3.2$  L min<sup>-1</sup>, corresponding to a residence time of 44, 30, or 27 s, respectively. Some of the experiments were carried out in the presence of water vapor or formic acid, both of which can act as SCI scavengers. Water vapor was added by bubbling a flow of clean air through nanopure water ( $18.2$  M $\Omega$  cm) into the flow reactor. The relative humidity of the airflow ( $\sim 75$  % RH) in the reactor was measured using a humidity probe (Vaisala, HMT234). Formic acid (Sigma-Aldrich,  $\geq 95$  %) was added to the reactor using the same method as for  $\alpha$ -cedrene.

The particle size distributions were measured at the outlet of the reactor using a scanning mobility particle sizer (SMPS, TSI), which is equipped with an electrostatic classifier (model 3080), a long differential mobility analyzer (model 3081) and a conden-

## Formation, composition, and phase of $\alpha$ -cedrene SOA

Y. Zhao et al.

Title Page

Abstract

Introduction

Conclusions

References

Tables

Figures



Back

Close

Full Screen / Esc

Printer-friendly Version

Interactive Discussion









## 2.3 SOA characterization

In both flow reactor and chamber experiments, aerosol samples were directed through a 10 cm monolith extruded carbon denuder (Novacarb<sup>TM</sup>; Mast Carbon, Ltd.) to remove the gas phase species prior to particle collection on the filter. No significant difference in particle size distribution was observed with or without the denuder. Blank experiments were also carried out under the same experimental conditions as the ozonolysis experiments but without adding O<sub>3</sub> to the flow reactor or the chamber.

### 2.3.1 ATR-FTIR measurements

The ATR crystal with impacted SOA was placed immediately into an ATR cell (volume ~ 2 cm<sup>3</sup>) located in the sampling compartment of a Nicolet 6700 FTIR spectrometer (Thermo Scientific). A flow of dry synthetic air at 100 mL min<sup>-1</sup> passed over the sample on the crystal. In some experiments, this flow first passed through a pen-ray mercury lamp, producing 8 ppm O<sub>3</sub>, in order to probe the possibility of secondary oxidation of SOA components by O<sub>3</sub>. Single beam spectra at a resolution of 4 cm<sup>-1</sup> (128 scans) were collected before and after impaction of SOA. The absorbance spectra of SOA on the crystal were derived from log<sub>10</sub>(S<sub>0</sub>/S<sub>1</sub>) where S<sub>0</sub> and S<sub>1</sub> represent the single beam spectra of the clean and SOA-covered crystal, respectively. The IR spectra of SOA were obtained over 20 h of air or O<sub>3</sub> exposure to study the evolution and evaporation of the impacted SOA during this period. In experiments performed in the presence of 2-EHN, the signal at 1280 cm<sup>-1</sup> was followed over time to investigate the evaporation of 2-EHN and determine its diffusion coefficient throughout the SOA matrix.

### 2.3.2 ESI-MS measurements

Extracts of both SOA and blank samples were analyzed by ESI-ToF-MS operated in either positive or negative ion mode. The operating conditions of this mass spectrometer were described previously (Zhao et al., 2015). Mass spectra were acquired in the

## Formation, composition, and phase of $\alpha$ -cedrene SOA

Y. Zhao et al.

Title Page

Abstract

Introduction

Conclusions

References

Tables

Figures

◀

▶

◀

▶

Back

Close

Full Screen / Esc

Printer-friendly Version

Interactive Discussion







**Formation,  
composition, and  
phase of  $\alpha$ -cedrene  
SOA**

Y. Zhao et al.

Title Page

Abstract

Introduction

Conclusions

References

Tables

Figures



Back

Close

Full Screen / Esc

Printer-friendly Version

Interactive Discussion



resent an increase or decrease respectively in the functional groups in SOA due to air exposure. There is a decrease in peaks at 3416, 1762, 1371 and 1076  $\text{cm}^{-1}$  and an increase in peaks at 1735, 1706, 1410 and in the 1100–1350  $\text{cm}^{-1}$  region. Note that there is no obvious change in the C-H peaks around 2957  $\text{cm}^{-1}$ , suggesting that evaporation of organic species from SOA during air exposure is not important. Therefore, the changes in SOA as indicated by the difference spectra are due to chemistry occurring in SOA during air exposure. One of the possible processes is the decomposition of oligomers that comprise a significant fraction of  $\alpha$ -cedrene SOA as discussed later. For example, decomposition of peroxyhemiacetals and aldol condensation products to their precursors can lead to the loss of O-H groups and concomitant formation of ketone/aldehyde C=O groups. The decomposition of oligomers in SOA was supported by ESI-MS measurements of SOA collected on Teflon filters and then exposed to a flow of clean dry air; thus the relative ion intensity of oligomers to LMW products in the mass spectrum of SOA extracted after 20 h of air exposure is  $\sim 15\%$  lower compared to that of SOA extracted immediately following collection. The difference spectrum of the SOA film exposed to clean humid air at 89% RH for 40 min (Fig. S3 in the Supplement) shows a broad band centered at 3426  $\text{cm}^{-1}$  and a narrow band at 1640  $\text{cm}^{-1}$  resulting from the stretching and bending vibration of adsorbed water respectively, with relative strength of stretching vs. bending of  $\sim 2$ . The absence of a negative peak at 1640  $\text{cm}^{-1}$  in the difference spectrum after dry air exposure as shown in Fig. 2b, therefore, suggests that the contribution of water to the loss in the O-H band at 3416  $\text{cm}^{-1}$  is minor and the decrease in this region must be due to a change in SOA components.

Figure 2c shows the difference spectrum of SOA upon exposure to 8 ppm  $\text{O}_3$  for 20 h which is very similar to the difference spectrum of SOA after 20 h of clean air exposure (Fig. 2b). This shows that the  $\alpha$ -cedrene SOA oxidation products are not reactive toward  $\text{O}_3$ , at least as detectable by changes in the infrared spectrum.



**Formation,  
composition, and  
phase of  $\alpha$ -cedrene  
SOA**

Y. Zhao et al.

Title Page

Abstract

Introduction

Conclusions

References

Tables

Figures



Back

Close

Full Screen / Esc

Printer-friendly Version

Interactive Discussion



The refractive index of  $\alpha$ -cedrene SOA is not known but a value of  $\sim 1.5$  is reasonable based on literature values for SOA from other biogenic organic oxidations (Lambe et al., 2013; Kim et al., 2014). The penetration depth of the IR beam at 1280 and 1635  $\text{cm}^{-1}$ , peaks which correspond to the absorption bands of organic nitrate as discussed below, is then calculated to be 0.52 and 0.41  $\mu\text{m}$  (Harrick, 1967), respectively, for SOA on a Ge crystal. This suggests that the entire depth of the SOA film on the ATR crystal can be probed reasonably well by the IR beam in the region of interest.

Figure 4a is a typical ATR-FTIR spectrum of  $\alpha$ -cedrene SOA formed in the presence of 2-EHN in the chamber under dry conditions. The spectrum is essentially the same as that of SOA formed without 2-EHN (Fig. 2a) except that there are two new bands at 1635 and 1280  $\text{cm}^{-1}$  resulting from the vibrations of nitrate (Socrates, 2001; Bruns et al., 2010; Perraud et al., 2012) when 2-EHN is present. Figure 4b shows the difference spectrum of SOA after exposure to a flow of clean dry air for 20 h. In addition to the spectral features similar to the difference spectrum of 2-EHN-free SOA (Fig. 2b), there is a small loss of nitrate peaks at 1635 and 1280  $\text{cm}^{-1}$ , indicating some evaporation of 2-EHN from SOA during air exposure. Figure 5 shows the temporal evolution of the integrated area of the nitrate peak at 1280  $\text{cm}^{-1}$  over 20 h of air exposure. It can be seen that after 20 h of air exposure, only  $\sim 27\%$  of 2-EHN evaporated from the SOA. This slow evaporation indicates that 2-EHN is incorporated in the bulk of the SOA, and that the SOA must be a high-viscosity semi-solid rather than a liquid where diffusion would be much more rapid (Shiraiwa et al., 2011; Koop et al., 2011).

The incorporation of high-volatility 2-EHN into the bulk of high-viscosity SOA is consistent with a condensation particle growth mechanism (Finlayson-Pitts and Pitts, 2000; Seinfeld and Pandis, 2006; Riipinen et al., 2011; Perraud et al., 2012), for which organic species condense kinetically onto the surface of pre-existing particles and become buried and incorporated into the bulk by incoming low volatility organics. It is important to note that in the ATR-FTIR spectrum (Fig. 4c) of  $\alpha$ -cedrene SOA formed without added 2-EHN in the chamber and then exposed to 20 ppm 2-EHN in the ATR cell for one hour, the absorption bands associated with organic nitrate at 1635 and

1280 cm<sup>-1</sup> are negligible. This observation suggests that the uptake of 2-EHN into or onto previously formed SOA is not important.

Assuming that the evaporation of 2-EHN is determined only by its diffusion in the film of SOA impacted on the ATR crystal and that the diffusion follows Fick's Law, for a film with uniform 2-EHN concentration ( $C_0$ ) at  $t = 0$  and zero concentration at the surface for  $t > 0$ , the total fraction ( $F$ ) of 2-EHN remaining in the film at time  $t$  can be expressed as (Crank, 1975; Mehrer, 2007)

$$F = \frac{8}{\pi^2} \sum_{j=0}^{\infty} \frac{1}{(2j+1)^2} \exp\left[-\frac{(2j+1)^2 \pi^2 D t}{4L^2}\right] \quad j = 0, 1, 2, \dots \quad (1)$$

In Eq. (1),  $D$  is the diffusion coefficient of 2-EHN in the SOA and  $L$  is the thickness of the SOA film on the ATR crystal. A best fit of the evaporation data of 2-EHN in Fig. 5 to Eq. (1) gives  $D/L^2 = 5.6 \times 10^{-5} \text{ min}^{-1}$ . With the SOA film thickness  $L$  of 0.54  $\mu\text{m}$  estimated above, the diffusion coefficient ( $D$ ) of 2-EHN in SOA is calculated to be  $3 \times 10^{-15} \text{ cm}^2 \text{ s}^{-1}$ , consistent with the  $D$  values of the order of  $\sim 10^{-15} \text{ cm}^2 \text{ s}^{-1}$  predicted from the time scale for evaporation combined with the estimated thickness of the SOA layer (Shiraiwa et al., 2011; Koop et al., 2011). The uncertainty in  $L$  of about a factor of two described above translates into an uncertainty in  $D$  of about a factor of four. However, this value for  $D$  is within the range of diffusion coefficients that would be expected in a highly viscous semi-solid matrix, i.e.,  $D = 10^{-10} - 10^{-20} \text{ cm}^2 \text{ s}^{-1}$  (Shiraiwa et al., 2011; Koop et al., 2011), confirming that  $\alpha$ -cedrene SOA is a high-viscosity semi-solid. However, because of their small sizes, these particles do not have enough momentum to bounce as they impact on the ATR crystal, as seen for larger SOA from  $\alpha$ -pinene oxidation in earlier studies (Kidd et al., 2014a, b). Recently, Saukko et al. (2012) and Pajunoja et al. (2015) reported the formation of semi-solid SOA from the oxidation of the sesquiterpene longifolene based on particle bounce measurements. However, to our knowledge, the present work shows the first measurement of the diffusion coefficient of an organic species in sesquiterpene SOA.

## Formation, composition, and phase of $\alpha$ -cedrene SOA

Y. Zhao et al.

[Title Page](#)[Abstract](#)[Introduction](#)[Conclusions](#)[References](#)[Tables](#)[Figures](#)[⏪](#)[⏩](#)[◀](#)[▶](#)[Back](#)[Close](#)[Full Screen / Esc](#)[Printer-friendly Version](#)[Interactive Discussion](#)



### 3.3 SOA composition

Figure 6 shows typical ESI+ and ESI− mass spectra of SOA formed from  $\alpha$ -cedrene ozonolysis in the flow reactor at 30 s reaction time. Ions in the mass range  $m/z$  220–350 correspond to low molecular weight (LMW) products derived directly from oxidation of  $\alpha$ -cedrene and retaining much of the structure of the parent compound (hereafter termed P1 products). Those with  $m/z > 420$  correspond to high molecular weight (HMW) products formed using two, three, or four P1 products (hereafter termed P2, P3, and P4 products, respectively) as building blocks. We try to avoid using the terms “dimer”, “trimer”, etc. which may imply simple combinations of smaller species whereas P2, P3, etc. are clearly complex combinations of different LMW products. The data presented in Fig. 6 suggest that P1 and P2 products comprise a dominant fraction of  $\alpha$ -cedrene SOA. Compared to the ESI+ spectrum, the corresponding ions in the ESI− spectrum are generally 24 Da lower in mass. This is consistent with the fact that the ions observed in the ESI+ mode are primarily sodium adducts while those in the ESI− mode are deprotonated ions with a predominant contribution from carboxylic acids.

Figure 7 shows the ESI mass spectra of polydisperse  $\alpha$ -cedrene SOA (size distributions are given in Fig. S1a) with geometric mean diameters of 15 and 23 nm formed in the flow reactor at the same concentrations of  $\alpha$ -cedrene and  $O_3$  but different reaction times (27 and 44 s) under dry conditions (Table 1, experiments FR1-FR2). In the smaller particles formed at shorter reaction times (Fig. 7a), P2 products account for a greater fraction of the total, and conversely, P1 products contribute more to larger particles formed at longer reaction times (Fig. 7b). Figure S4 in the Supplement shows additional ESI mass spectra of polydisperse  $\alpha$ -cedrene SOA particles of different geometric mean diameters (13, 18, and 26 nm) formed in the flow reactor at the same reaction time (30 s) but different concentrations of  $\alpha$ -cedrene under dry conditions (Table 1, experiments FR3-FR5). A similar size-dependent distribution of P1 and P2 products is observed. These results suggest that P2 products (particularly those at  $m/z$  481–543)

## Formation, composition, and phase of $\alpha$ -cedrene SOA

Y. Zhao et al.

Title Page

Abstract

Introduction

Conclusions

References

Tables

Figures



Back

Close

Full Screen / Esc

Printer-friendly Version

Interactive Discussion









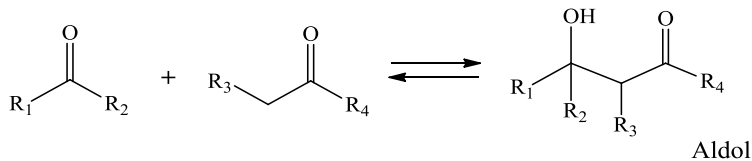


radicals via the vinyl hydroperoxide (VHP) channel. The conversion of  $RO_2$  to alkoxy (RO) radicals and the subsequent intramolecular H-abstraction/ $O_2$  addition lead again to  $RO_2$  radicals, which can further undergo similar reactions to form  $RO_2$  radicals with higher oxygen content. Termination reactions with  $RO_2$  or  $HO_2$  radicals lead to the formation of the newly observed products.

While accurate mass data of these products (Table 2) agree well with the proposed structures, there may be additional structures and reaction pathways in the formation of the P1 products at  $m/z$  305–323 via the VHP channel of CIs that contribute to these peaks. For example, because of their large carbon skeleton, RO radicals may have multiple isomerization pathways to form different structures with the same elemental composition.

### 3.3.2 P2 products

Table 2 gives the accurate masses and elemental formulae of the most abundant P2 products as labeled in the ESI mass spectra (Fig. 6a). Figure 10 shows the proposed potential structures of these products based on their accurate mass data and ESI- $MS^2$  spectra (Fig. S10; see Supplement for the detailed discussion). These structures include aldol condensation products (formed from the reaction of two carbonyl compounds, Reaction R1), peroxyhemiacetals (formed from the reaction of a carbonyl compound and an organic hydroperoxide, Reaction R2), and esters (formed from the reaction of a carboxylic acid with an alcohol, Reaction R3), with the building blocks being the P1 products typically observed in the SOA.



(R1)

35000

ACPD

15, 34981–35034, 2015

## Formation, composition, and phase of $\alpha$ -cedrene SOA

Y. Zhao et al.

Title Page

Abstract

Introduction

Conclusions

References

Tables

Figures

◀

▶

◀

▶

Back

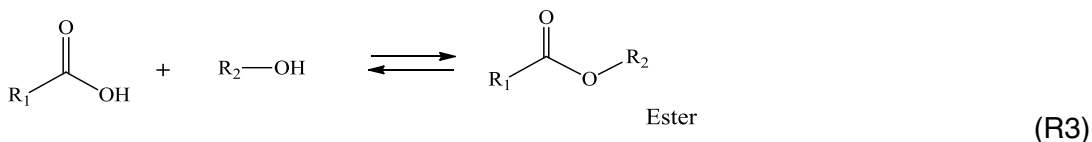
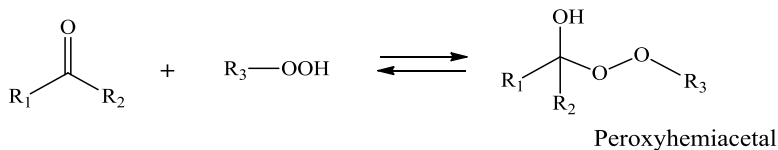
Close

Full Screen / Esc

Printer-friendly Version

Interactive Discussion





5 Aldol condensation products and peroxyhemiacetals are the most commonly identified structures. Of 17 proposed structures for these P2 products, ten are aldol condensation products and five are peroxyhemiacetals. Except for products P2-481 and P2-497 that are identified as aldol condensation products, other P2 products may have contributions from multiple structures. For example, product P2-511 may have contributions from both aldol condensation products and esters, and products P2-513, P2-527, 10 and P2-543 may have contributions from both aldol condensation products and peroxyhemiacetals. Although no detailed data concerning the formation of such HMW products during sesquiterpene ozonolysis are available in the literature, a number of laboratory and field studies have found that aldol condensation products, peroxyhemiacetals, and esters are the major HMW products detected in the SOA formed from 15 ozonolysis of monoterpenes (e.g.,  $\alpha$ -pinene and  $\beta$ -pinene) (Hoffmann et al., 1998; Tolocka et al., 2004; Docherty et al., 2005; Muller et al., 2008, 2009; Heaton et al., 2009; Gao et al., 2010; Yasmeen et al., 2010; Hall and Johnston, 2012; Kristensen et al., 2013, 2014; Witkowski and Gierczak, 2014; X. Zhang et al., 2015). Formation of such products has traditionally been thought to occur via acid-catalyzed reactions (Reactions R1–R3) in the condensed phase (Kroll and Seinfeld, 2008; Hallquist et al., 20

35001

**Formation,  
composition, and  
phase of  $\alpha$ -cedrene  
SOA**

Y. Zhao et al.

Title Page

Abstract

Introduction

Conclusions

References

Tables

Figures

◀

▶

◀

▶

Back

Close

Full Screen / Esc

Printer-friendly Version

Interactive Discussion





**Formation,  
composition, and  
phase of  $\alpha$ -cedrene  
SOA**

Y. Zhao et al.

Title Page

Abstract

Introduction

Conclusions

References

Tables

Figures

◀

▶

◀

▶

Back

Close

Full Screen / Esc

Printer-friendly Version

Interactive Discussion



CH<sub>2</sub>OO, if the rate constants for the latter are representative in a relative sense, the ratio of the rates for reaction of the  $\alpha$ -cedrene CI with formic acid and water dimer relative to water monomer are  $\sim 240 : 18 : 1$  under our experimental conditions ( $3.7 \times 10^{14}$  HCOOH cm<sup>-3</sup>,  $4.8 \times 10^{17}$  H<sub>2</sub>O cm<sup>-3</sup> and  $5.1 \times 10^{14}$  (H<sub>2</sub>O)<sub>2</sub> cm<sup>-3</sup>, based on a water equilibrium constant of 0.0536 atm<sup>-1</sup> (Ruscic, 2013)). Thus, it is not surprising that formic acid has a much greater impact than water. Furthermore, the large effects of formic acid further support the importance of the  $\alpha$ -cedrene CI in SOA formation. These impacts of water and formic acid are in agreement with those reported by Yao et al. (2014) who reported a similar quenching effect of added acetic acid on particle formation in the  $\alpha$ -cedrene ozonolysis, but relatively little impact of water vapor.

Figure 12a and b shows the ESI mass spectra of  $\alpha$ -cedrene SOA formed in the flow reactor without and with added water vapor, respectively. There are no significant differences in product distribution with and without added water vapor. In addition, ESI-MS<sup>2</sup> measurements show that typical P1 and P2 products as labeled in both mass spectra have very similar MS<sup>2</sup> spectra, suggesting that the product composition is not impacted by the presence of water. Measurements of the chamber SOA by AMS (see Fig. S11 in the Supplement) also did not show significant differences in the particle mass spectra upon water addition. On the other hand, Fig. 12c shows the ESI mass spectra of SOA formed in the presence of 15 ppm formic acid. The formation of HMW products is significantly reduced as are the number of peaks in the P1 product region. However, P1 products at  $m/z$  259, 275, and 291, as well as P2 products, for example, at  $m/z$  527, 543, and 559, are still evident. All of these P1 products have very similar MS<sup>2</sup> spectra (and thus likely similar structures) to those formed in the absence of formic acid. In contrast, P2 products at  $m/z$  527 and 543 show significantly different MS<sup>2</sup> spectra compared to those obtained without added formic acid.

Yao et al. (2014) reported an increase in the formation of  $\alpha$ -cedronaldehyde in the presence of acetic acid, consistent with an increase in the present studies in the relative abundance of the P1 product at  $m/z$  259 assigned to  $\alpha$ -cedronaldehyde when formic acid was added (Fig. 12c). The reaction of  $\alpha$ -cedrene SCI with formic acid is expected



to form  $\alpha$ -formyloxy hydroperoxide (MW 298 Da), which is believed to contribute to SOA growth. While the corresponding sodium adduct at  $m/z$  321 is not observed in the mass spectrum, this is not surprising as hydroperoxides are likely to undergo decomposition during SOA sampling and analysis (Witkowski and Gierczak, 2013).

5 Comparison of Fig. 12c to Fig. 12a shows that HMW products (P2–P4) formed with added formic acid are relatively less important than those produced in the absence of formic acid. Combined with the smaller number concentration (Fig. 11), the data suggest that HMW products must be important in new particle formation. As fewer particles are formed with the addition of formic acid, more P1 products are available for  
10 each particle to grow to larger sizes.

### 3.5 Mechanisms

The size-dependent composition of  $\alpha$ -cedrene SOA and the effect of SCI scavengers on particle formation suggest that HMW products (P2–P4) play an important role in the initial stages of particle formation. This is consistent with earlier suggestions in simpler systems that higher molecular weight products of alkene ozonolysis are primarily  
15 responsible for nucleation, while many different products from low to high molecular weight can contribute to growth (Lee and Kamens, 2005; Sadezky et al., 2008; Winkler et al., 2012; Zhao et al., 2013; Ehn et al., 2014; Kidd et al., 2014a; Zhao et al., 2015; X. Zhang et al., 2015). Bonn and Moortgat (2003) estimated an upper limit for the saturated vapor pressure ( $P_{\text{sat}}$ ) of nucleating species produced from sesquiterpene  
20 ozonolysis to be  $1.2 \times 10^{-13}$  atm. Donahue et al. (2013) also suggested that organic vapors with  $P_{\text{sat}} < 10^{-13}$  atm may contribute to particle nucleation. The  $P_{\text{sat}}$  of typical P1 products, as well as the P2 products (e.g., ester and peroxyhemiacetal) are estimated by averaging the predictions (see Table S1 in the Supplement) from two group contribution methods, SIMPOL.1 (Pankow and Asher, 2008) and EVAPORATION (Compernelle  
25 et al., 2011), and are shown in Fig. 13. The  $P_{\text{sat}}$  for the P2 products are 3–6 orders of magnitude lower than the suggested nucleation threshold, consistent with their important contributions to initial particle formation. The newly observed products (P1-321

## Formation, composition, and phase of $\alpha$ -cedrene SOA

Y. Zhao et al.

Title Page

Abstract

Introduction

Conclusions

References

Tables

Figures



Back

Close

Full Screen / Esc

Printer-friendly Version

Interactive Discussion





and P1-323) also have vapor pressures lower than the nucleation threshold and thus may in principle also contribute to nucleation. In contrast, the smaller, more volatile P1 products will mainly contribute to particle growth, as suggested by their relatively larger abundance in ESI mass spectra of larger particles (Figs. 7 and S4).

Compared to P2 products at  $m/z$  481–543, those with  $m/z$  values  $> 543$  are significantly less important in the flow reactor SOA (geometric mean diameter 13–26 nm), but contribute a greater fraction to total P2 products in the chamber SOA (geometric mean diameter 66 nm). This suggests that the larger P2 products ( $> m/z$  543) play an important role in particle growth and may be formed mainly via condensed phase reactions of P1 products in the SOA.

Elemental analysis of SOA from chamber experiments using AMS results in an average O/C ratio of  $0.34 \pm 0.03$  ( $1\sigma$ ) and H/C ratio of  $1.51 \pm 0.02$ . These values are within the range given for P1 products detected by ESI-MS (Table 2) and are consistent with our observation that P1 products predominantly contribute to particle growth. Along with the potential mechanisms discussed above to explain the formation of observed P1 and P2 products and their contribution to particle formation and growth, another mechanism considered for particle formation and growth is the production of extremely low-volatility organic compounds (ELVOCs), which was proposed to occur via sequential intramolecular hydrogen abstraction/O<sub>2</sub> addition of RO<sub>2</sub> radicals (Vereecken et al., 2007; Crouse et al., 2013; Ehn et al., 2014; Rissanen et al., 2015) and shown to play an important role in particle formation and growth from monoterpene oxidation (Zhao et al., 2013; Ehn et al., 2014; Jokinen et al., 2015). Because of the high oxygen content in ELVOCs, particles formed from these compounds are expected to have high O/C ratios. The ELVOC mechanism cannot be ruled out as being involved in initial particle formation during  $\alpha$ -cedrene ozonolysis. However, based on the O/C ratios measured for chamber SOA, it is unlikely to be a dominant contributor to total particle mass in this system. Measurements by AMS are not possible for the flow reactor experiments as the particles are too small to be efficiently transmitted into the AMS.

## Formation, composition, and phase of $\alpha$ -cedrene SOA

Y. Zhao et al.

Title Page

Abstract

Introduction

Conclusions

References

Tables

Figures



Back

Close

Full Screen / Esc

Printer-friendly Version

Interactive Discussion



**Formation,  
composition, and  
phase of  $\alpha$ -cedrene  
SOA**

Y. Zhao et al.

Title Page

Abstract

Introduction

Conclusions

References

Tables

Figures



Back

Close

Full Screen / Esc

Printer-friendly Version

Interactive Discussion



It is clear from the impact of formic acid on particle formation that the SCI plays a key role in forming the HMW products and new particles. In the case of the *trans*-3-hexene ozonolysis (Sadezky et al., 2008; Zhao et al., 2015), the composition of the SOA clearly showed evidence for oligomer formation from the sequential reaction of RO<sub>2</sub> radicals with SCI, leading to ESI mass spectra that showed the repeat unit of oligomers corresponding to SCI. A search for similar products in the  $\alpha$ -cedrene reaction was not successful, indicating that while this may contribute, other mechanisms are more important (Zhao et al., 2015). This is not surprising, given the number of potential reaction paths for the SCI from  $\alpha$ -cedrene (e.g. Fig. S9) and the large number of low volatility products that can quickly contribute to growth and the SOA composition once nucleation has occurred.

The incorporation of 2-EHN into SOA and its very slow evaporation back out (Figs. 4 and 5) is consistent with a condensation type of growth mechanism (Finlayson-Pitts and Pitts, 2000; Seinfeld and Pandis, 2006) in which incorporation into particles depends on the collision frequency of the gas with the particle surface and the magnitude of the uptake coefficient (Perraud et al., 2012). Such a growth mechanism is characteristic of highly viscous SOA, in contrast to an equilibrium mechanism that applies for low-viscosity liquid particles. This result also suggests that growth will occur not only via low volatility products but also via uptake of higher volatility species such as the smaller P1 products identified here.

## 4 Summary

The present study examines the phase state and mechanisms of formation and growth of SOA from ozonolysis of  $\alpha$ -cedrene. The SOA is characterized to be a high-viscosity semi-solid, with an estimated diffusion coefficient of  $3 \times 10^{-15} \text{ cm}^2 \text{ s}^{-1}$  for 2-EHN that was incorporated into the SOA during ozonolysis. High molecular weight products, tentatively identified mainly as aldol condensation products, peroxyhemiacetals, and esters, comprise a significant fraction of SOA. The size-dependent distribution of these

products in the SOA as well as their positive correlation with new particle formation suggests that they are responsible for initial particle formation, in contrast to lower molecular weight (P1) products that mainly contribute to particle growth via a kinetic condensation mechanism.

Mechanisms of ozonolysis of alkenes and in particular, the pathways that lead to SOA formation are highly dependent on the size and structure of the parent alkene. However, in all cases stabilized Criegee intermediates play a key role. For example, SOA generated from ozonolysis of small alkenes such as *trans*-3-hexene is primarily composed of oligomers formed from the sequential addition of SCI to RO<sub>2</sub> radicals (Sadezky et al., 2008; Zhao et al., 2015). For larger alkenes, such as  $\alpha$ -cedrene, the SCI react via multiple pathways, leading to a variety of low volatility products (e.g., P2 and newly observed P1 products) that can nucleate on their own to form new particles. There is yet a third group of alkenes with intermediate molecular sizes such as monoterpenes, for which the major first generation ozonolysis products do not have low enough volatilities to nucleate on their own (Hallquist et al., 2009) and therefore the ELVOC mechanism, despite the small yields (a few percent, Jokinen et al., 2015), may play a more dominant role (Zhao et al., 2013; Ehn et al., 2014). The dependence of phase, composition, and mechanisms for particle formation and growth should be taken into account in atmospheric models of the formation and impacts of SOA on visibility, human health, and climate.

**The Supplement related to this article is available online at doi:10.5194/acpd-15-34981-2015-supplement.**

*Acknowledgements.* This work was supported by the National Science Foundation (Grants #1207112) and the NSF Major Research Instrumentation (MRI) program (Grant # 0923323 and 1337080). The authors are grateful to John Greaves, Beniam Berhane, and Shirin Sorooshian for their help with accurate mass measurements.

**Formation,  
composition, and  
phase of  $\alpha$ -cedrene  
SOA**

Y. Zhao et al.

Title Page

Abstract

Introduction

Conclusions

References

Tables

Figures

◀

▶

◀

▶

Back

Close

Full Screen / Esc

Printer-friendly Version

Interactive Discussion



## References

- Abramson, E., Imre, D., Beranek, J., Wilson, J., and Zelenyuk, A.: Experimental determination of chemical diffusion within secondary organic aerosol particles, *Phys. Chem. Chem. Phys.*, 15, 2983–2991, doi:10.1039/C2cp44013j, 2013.
- 5 Alfarra, M. R., Hamilton, J. F., Wyche, K. P., Good, N., Ward, M. W., Carr, T., Barley, M. H., Monks, P. S., Jenkin, M. E., Lewis, A. C., and McFiggans, G. B.: The effect of photochemical ageing and initial precursor concentration on the composition and hygroscopic properties of  $\beta$ -caryophyllene secondary organic aerosol, *Atmos. Chem. Phys.*, 12, 6417–6436, doi:10.5194/acp-12-6417-2012, 2012.
- 10 Anglada, J. M., Gonzalez, J., and Torrent-Sucarrat, M.: Effects of the substituents on the reactivity of carbonyl oxides, a theoretical study on the reaction of substituted carbonyl oxides with water, *Phys. Chem. Chem. Phys.*, 13, 13034–13045, doi:10.1039/c1cp20872a, 2011.
- Bateman, A. P., Bertram, A. K., and Martin, S. T.: Hygroscopic influence on the semisolid-to-liquid transition of secondary organic materials, *J. Phys. Chem. A*, 119, 4386–4395, doi:10.1021/jp508521c, 2015.
- 15 Berndt, T., Kaethner, R., Voigtlander, J., Stratmann, F., Pfeifle, M., Reichle, P., Sipila, M., Kulmala, M., and Olzmann, M.: Kinetics of the unimolecular reaction of  $\text{CH}_2\text{OO}$  and the bimolecular reactions with the water monomer, acetaldehyde and acetone under atmospheric conditions, *Phys. Chem. Chem. Phys.*, 17, 19862–19873, doi:10.1039/c5cp02224j, 2015.
- 20 Birdsall, A. W., Zentner, C. A., and Elrod, M. J.: Study of the kinetics and equilibria of the oligomerization reactions of 2-methylglyceric acid, *Atmos. Chem. Phys.*, 13, 3097–3109, doi:10.5194/acp-13-3097-2013, 2013.
- Bones, D. L., Reid, J. P., Lienhard, D. M., and Krieger, U. K.: Comparing the mechanism of water condensation and evaporation in glassy aerosol, *P. Natl. Acad. Sci. USA*, 109, 11613–11618, 2012.
- 25 Bonn, B. and Moortgat, G. K.: Sesquiterpene ozonolysis: origin of atmospheric new particle formation from biogenic hydrocarbons, *Geophys. Res. Lett.*, 30, 1585, doi:10.1029/2003GL017000, 2003.
- Bonn, B., Kulmala, M., Riipinen, I., Sihto, S. L., and Ruuskanen, T. M.: How biogenic terpenes govern the correlation between sulfuric acid concentrations and new particle formation, *J. Geophys. Res.*, 113, D12209, doi:10.1029/2007jd009327, 2008.
- 30

**Formation,  
composition, and  
phase of  $\alpha$ -cedrene  
SOA**

Y. Zhao et al.

Title Page

Abstract

Introduction

Conclusions

References

Tables

Figures

◀

▶

◀

▶

Back

Close

Full Screen / Esc

Printer-friendly Version

Interactive Discussion



**Formation,  
composition, and  
phase of  $\alpha$ -cedrene  
SOA**

Y. Zhao et al.

Title Page

Abstract

Introduction

Conclusions

References

Tables

Figures



Back

Close

Full Screen / Esc

Printer-friendly Version

Interactive Discussion



Bouvier-Brown, N. C., Goldstein, A. H., Gilman, J. B., Kuster, W. C., and de Gouw, J. A.: In-situ ambient quantification of monoterpenes, sesquiterpenes, and related oxygenated compounds during BEARPEX 2007: implications for gas- and particle-phase chemistry, *Atmos. Chem. Phys.*, 9, 5505–5518, doi:10.5194/acp-9-5505-2009, 2009.

5 Boy, M., Karl, T., Turnipseed, A., Mauldin, R. L., Kosciuch, E., Greenberg, J., Rathbone, J., Smith, J., Held, A., Barsanti, K., Wehner, B., Bauer, S., Wiedensohler, A., Bonn, B., Kulmala, M., and Guenther, A.: New particle formation in the Front Range of the Colorado Rocky Mountains, *Atmos. Chem. Phys.*, 8, 1577–1590, doi:10.5194/acp-8-1577-2008, 2008.

10 Bruns, E. A., Perraud, V., Zelenyuk, A., Ezell, M. J., Johnson, S. N., Yu, Y., Imre, D., Finlayson-Pitts, B. J., and Alexander, M. L.: Comparison of FTIR and particle mass spectrometry for the measurement of particulate organic nitrates, *Environ. Sci. Technol.*, 44, 1056–1061, doi:10.1021/Es9029864, 2010.

15 Canagaratna, M. R., Jimenez, J. L., Kroll, J. H., Chen, Q., Kessler, S. H., Massoli, P., Hildebrandt Ruiz, L., Fortner, E., Williams, L. R., Wilson, K. R., Surratt, J. D., Donahue, N. M., Jayne, J. T., and Worsnop, D. R.: Elemental ratio measurements of organic compounds using aerosol mass spectrometry: characterization, improved calibration, and implications, *Atmos. Chem. Phys.*, 15, 253–272, doi:10.5194/acp-15-253-2015, 2015.

20 Cappa, C. D. and Wilson, K. R.: Evolution of organic aerosol mass spectra upon heating: implications for OA phase and partitioning behavior, *Atmos. Chem. Phys.*, 11, 1895–1911, doi:10.5194/acp-11-1895-2011, 2011.

25 Chan, M. N., Surratt, J. D., Chan, A. W. H., Schilling, K., Offenberg, J. H., Lewandowski, M., Edney, E. O., Kleindienst, T. E., Jaoui, M., Edgerton, E. S., Tanner, R. L., Shaw, S. L., Zheng, M., Knipping, E. M., and Seinfeld, J. H.: Influence of aerosol acidity on the chemical composition of secondary organic aerosol from beta;-caryophyllene, *Atmos. Chem. Phys.*, 11, 1735–1751, doi:10.5194/acp-11-1735-2011, 2011.

Chan, M. N., Zhang, H. F., Goldstein, A. H., and Wilson, K. R.: Role of water and phase in the heterogeneous oxidation of solid and aqueous succinic acid aerosol by hydroxyl radicals, *J. Phys. Chem. C*, 118, 28978–28992, doi:10.1021/jp5012022, 2014.

30 Chao, W., Hsieh, J. T., Chang, C. H., and Lin, J. J. M.: Direct kinetic measurement of the reaction of the simplest Criegee intermediate with water vapor, *Science*, 347, 751–754, doi:10.1126/science.1261549, 2015.

**Formation,  
composition, and  
phase of  $\alpha$ -cedrene  
SOA**

Y. Zhao et al.

Title Page

Abstract

Introduction

Conclusions

References

Tables

Figures

◀

▶

◀

▶

Back

Close

Full Screen / Esc

Printer-friendly Version

Interactive Discussion



Chen, Q., Li, Y. L., McKinney, K. A., Kuwata, M., and Martin, S. T.: Particle mass yield from *beta*-caryophyllene ozonolysis, *Atmos. Chem. Phys.*, 12, 3165–3179, doi:10.5194/acp-12-3165-2012, 2012.

Cody, R. B., Laramée, J. A., and Durst, H. D.: Versatile new ion source for the analysis of materials in open air under ambient conditions, *Anal. Chem.*, 77, 2297–2302, doi:10.1021/ac050162j, 2005.

Compernelle, S., Ceulemans, K., and Müller, J.-F.: EVAPORATION: a new vapour pressure estimation method for organic molecules including non-additivity and intramolecular interactions, *Atmos. Chem. Phys.*, 11, 9431–9450, doi:10.5194/acp-11-9431-2011, 2011.

Crank, J.: *The Mathematics of Diffusion*, 2nd edn., Clarendon Press, Oxford, UK, 1975.

Crouse, J. D., Nielsen, L. B., Jorgensen, S., Kjaergaard, H. G., and Wennberg, P. O.: Autoxidation of organic compounds in the atmosphere, *J. Phys. Chem. Lett.*, 4, 3513–3520, 2013.

DeCarlo, P. F., Kimmel, J. R., Trimborn, A., Northway, M. J., Jayne, J. T., Aiken, A. C., Gonin, M., Fuhrer, K., Horvath, T., Docherty, K. S., Worsnop, D. R., and Jimenez, J. L.: Field-deployable, high-resolution, time-of-flight aerosol mass spectrometer, *Anal. Chem.*, 78, 8281–8289, 2006.

DePalma, J. W., Horan, A. J., Hall, W. A., and Johnston, M. V.: Thermodynamics of oligomer formation: implications for secondary organic aerosol formation and reactivity, *Phys. Chem. Chem. Phys.*, 15, 6935–6944, 2013.

Ding, X., He, Q. F., Shen, R. Q., Yu, Q. Q., and Wang, X. M.: Spatial distributions of secondary organic aerosols from isoprene, monoterpenes, beta-caryophyllene, and aromatics over China during summer, *J. Geophys. Res.*, 119, 11877–11891, doi:10.1002/2014jd021748, 2014.

Docherty, K. S., Wu, W., Lim, Y. B., and Ziemann, P. J.: Contributions of organic peroxides to secondary aerosol formed from reactions of monoterpenes with O<sub>3</sub>, *Environ. Sci. Technol.*, 39, 4049–4059, 2005.

Donahue, N. M., Drozd, G. T., Epstein, S. A., Presto, A. A., and Kroll, J. H.: Adventures in ozoneland: down the rabbit-hole, *Phys. Chem. Chem. Phys.*, 13, 10848–10857, doi:10.1039/c0cp02564j, 2011.

Donahue, N. M., Ortega, I. K., Chuang, W., Riipinen, I., Riccobono, F., Schobesberger, S., Dommen, J., Baltensperger, U., Kulmala, M., Worsnop, D. R., and Vehkamäki, H.: How do organic vapors contribute to new-particle formation?, *Faraday Discuss.*, 165, 91–104, doi:10.1039/c3fd00046j, 2013.

**Formation,  
composition, and  
phase of  $\alpha$ -cedrene  
SOA**

Y. Zhao et al.

Title Page

Abstract

Introduction

Conclusions

References

Tables

Figures

◀

▶

◀

▶

Back

Close

Full Screen / Esc

Printer-friendly Version

Interactive Discussion



- Duhl, T. R., Helmig, D., and Guenther, A.: Sesquiterpene emissions from vegetation: a review, *Biogeosciences*, 5, 761–777, doi:10.5194/bg-5-761-2008, 2008.
- Ehn, M., Thornton, J. A., Kleist, E., Sipila, M., Junninen, H., Pullinen, I., Springer, M., Rubach, F., Tillmann, R., Lee, B., Lopez-Hilfiker, F., Andres, S., Acir, I. H., Rissanen, M., Jokinen, T., Schobesberger, S., Kangasluoma, J., Kontkanen, J., Nieminen, T., Kurten, T., Nielsen, L. B., Jorgensen, S., Kjaergaard, H. G., Canagaratna, M., Dal Maso, M., Berndt, T., Petaja, T., Wahner, A., Kerminen, V. M., Kulmala, M., Worsnop, D. R., Wildt, J., and Mentel, T. F.: A large source of low-volatility secondary organic aerosol, *Nature*, 506, 476–479, 2014.
- Finlayson-Pitts, B. J. and Pitts, J. N.: *Chemistry of the upper and lower atmosphere: theory, experiments, and applications*, Academic Press, San Diego, USA, 2000.
- Gao, Y. Q., Hall, W. A., and Johnston, M. V.: Molecular composition of monoterpene secondary organic aerosol at low mass loading, *Environ. Sci. Technol.*, 44, 7897–7902, doi:10.1021/Es101861k, 2010.
- Goldstein, A. H. and Galbally, I. E.: Known and unexplored organic constituents in the earth's atmosphere, *Environ. Sci. Technol.*, 41, 1514–1521, doi:10.1021/Es072476p, 2007.
- Guenther, A., Hewitt, C. N., Erickson, D., Fall, R., Geron, C., Graedel, T., Harley, P., Klinger, L., Lerdau, M., McKay, W. A., Pierce, T., Scholes, B., Steinbrecher, R., Tallamraju, R., Taylor, J., and Zimmerman, P.: A global-model of natural volatile organic compound emissions, *J. Geophys. Res.*, 100, 8873–8892, doi:10.1029/94jd02950, 1995.
- Hall, W. A. and Johnston, M. V.: Oligomer formation pathways in secondary organic aerosol from MS and MS/MS measurements with high mass accuracy and resolving power, *J. Am. Soc. Mass Spectr.*, 23, 1097–1108, 2012.
- Hallquist, M., Wenger, J. C., Baltensperger, U., Rudich, Y., Simpson, D., Claeys, M., Dommen, J., Donahue, N. M., George, C., Goldstein, A. H., Hamilton, J. F., Herrmann, H., Hoffmann, T., Iinuma, Y., Jang, M., Jenkin, M. E., Jimenez, J. L., Kiendler-Scharr, A., Maenhaut, W., McFiggans, G., Mentel, Th. F., Monod, A., Prévôt, A. S. H., Seinfeld, J. H., Surratt, J. D., Szmigielski, R., and Wildt, J.: The formation, properties and impact of secondary organic aerosol: current and emerging issues, *Atmos. Chem. Phys.*, 9, 5155–5236, doi:10.5194/acp-9-5155-2009, 2009.
- Harrick, N. J.: *Internal Reflection Spectroscopy*, Interscience Publishers, New York, USA, 1967.



**Formation,  
composition, and  
phase of  $\alpha$ -cedrene  
SOA**

Y. Zhao et al.

Title Page

Abstract

Introduction

Conclusions

References

Tables

Figures



Back

Close

Full Screen / Esc

Printer-friendly Version

Interactive Discussion



Heaton, K. J., Sleighter, R. L., Hatcher, P. G., Hall, W. A., and Johnston, M. V.: Composition domains in monoterpene secondary organic aerosol, *Environ. Sci. Technol.*, 43, 7797–7802, 2009.

Helmig, D., Ortega, J., Duhl, T., Tanner, D., Guenther, A., Harley, P., Wiedinmyer, C., Milford, J., and Sakulyanontvittaya, T.: Sesquiterpene emissions from pine trees – identifications, emission rates and flux estimates for the contiguous United States, *Environ. Sci. Technol.*, 41, 1545–1553, doi:10.1021/Es0618907, 2007.

Hodas, N., Zuend, A., Mui, W., Flagan, R. C., and Seinfeld, J. H.: Influence of particle-phase state on the hygroscopic behavior of mixed organic–inorganic aerosols, *Atmos. Chem. Phys.*, 15, 5027–5045, doi:10.5194/acp-15-5027-2015, 2015.

Hoffmann, T., Odum, J. R., Bowman, F., Collins, D., Klockow, D., Flagan, R. C., and Seinfeld, J. H.: Formation of organic aerosols from the oxidation of biogenic hydrocarbons, *J. Atmos. Chem.*, 26, 189–222, doi:10.1023/A:1005734301837, 1997.

Hoffmann, T., Bandur, R., Marggraf, U., and Lindscheid, M.: Molecular composition of organic aerosols formed in the alpha-pinene/O<sub>3</sub> reaction: implications for new particle formation processes, *J. Geophys. Res.*, 103, 25569–25578, 1998.

Hu, D., Bian, Q., Li, T. W. Y., Lau, A. K. H., and Yu, J. Z.: Contributions of isoprene, monoterpenes, beta-caryophyllene, and toluene to secondary organic aerosols in Hong Kong during the summer of 2006, *J. Geophys. Res.*, 113, D22206, doi:10.1029/2008jd010437, 2008.

IPCC 2013: Climate Change: Summary for Policymakers. The Physical Science Basis, Working Group I Contribution to the Fifth Assessment Report of the Intergovernmental Panel on Climate Change, edited by: Stocker, T. F., Qin, D., Plattner, G.-K., Tignor, M., Allen, S. K., Boschung, J., Nauels, A., Xia, Y., Bex, V., and Midgley, P. M., Cambridge University Press, Cambridge, UK, New York, NY, USA, 2013.

Jaoui, M., Sexton, K. G., and Kamens, R. M.: Reaction of alpha-cedrene with ozone: mechanism, gas and particulate products distribution, *Atmos. Environ.*, 38, 2709–2725, 2004.

Jaoui, M., Kleindienst, T. E., Docherty, K. S., Lewandowski, M., and Offenberg, J. H.: Secondary organic aerosol formation from the oxidation of a series of sesquiterpenes: alpha-cedrene, beta-caryophyllene, alpha-humulene and alpha-farnesene with O<sub>3</sub>, OH and NO<sub>3</sub> radicals, *Environ. Chem.*, 10, 178–193, doi:10.1071/En13025, 2013.

Jokinen, T., Berndt, T., Makkonen, R., Kerminen, V. M., Junninen, H., Paasonen, P., Stratmann, F., Herrmann, H., Guenther, A. B., Worsnop, D. R., Kulmala, M., Ehn, M., and Sipilä, M.: Production of extremely low volatile organic compounds from biogenic emissions:





**Formation,  
composition, and  
phase of  $\alpha$ -cedrene  
SOA**

Y. Zhao et al.

Title Page

Abstract

Introduction

Conclusions

References

Tables

Figures

◀

▶

◀

▶

Back

Close

Full Screen / Esc

Printer-friendly Version

Interactive Discussion



- Lambe, A. T., Cappa, C. D., Massoli, P., Onasch, T. B., Forestieri, S. D., Martin, A. T., Cummings, M. J., Croasdale, D. R., Brune, W. H., Worsnop, D. R., and Davidovits, P.: Relationship between oxidation level and optical properties of secondary organic aerosol, *Environ. Sci. Technol.*, 47, 6349–6357, 2013.
- 5 Lee, A., Goldstein, A. H., Keywood, M. D., Gao, S., Varutbangkul, V., Bahreini, R., Ng, N. L., Flagan, R. C., and Seinfeld, J. H.: Gas-phase products and secondary aerosol yields from the ozonolysis of ten different terpenes, *J. Geophys. Res.*, 111, D07302, doi:10.1029/2005JD006437, 2006.
- 10 Lee, C. T. and Kamens, R. M.: Particle nucleation from the reaction of  $\alpha$ -pinene and  $O_3$ , *Atmos. Environ.*, 39, 6822–6832, 2005.
- Lewis, T. R., Blitz, M. A., Heard, D. E., and Seakins, P. W.: Direct evidence for a substantive reaction between the Criegee intermediate,  $CH_2OO$ , and the water vapour dimer, *Phys. Chem. Chem. Phys.*, 17, 4859–4863, doi:10.1039/c4cp04750h, 2015.
- 15 Li, Y. J., Chen, Q., Guzman, M. I., Chan, C. K., and Martin, S. T.: Second-generation products contribute substantially to the particle-phase organic material produced by beta;-caryophyllene ozonolysis, *Atmos. Chem. Phys.*, 11, 121–132, doi:10.5194/acp-11-121-2011, 2011.
- Lignell, H., Hinks, M. L., and Nizkorodov, S. A.: Exploring matrix effects on photochemistry of organic aerosols, *P. Natl. Acad. Sci. USA*, 111, 13780–13785, 2014.
- 20 Mauderly, J. L. and Chow, J. C.: Health effects of organic aerosols, *Inhal. Toxicol.*, 20, 257–288, doi:10.1080/08958370701866008, 2008.
- Mehrer, H.: *Diffusion in Solids: Fundamentals, Methods, Materials, Diffusion-Controlled Processes*, Springer Series in Solid State Science, 155, Springer, Berlin, Germany, New York, USA, 2007.
- 25 Mikhailov, E., Vlasenko, S., Martin, S. T., Koop, T., and Pöschl, U.: Amorphous and crystalline aerosol particles interacting with water vapor: conceptual framework and experimental evidence for restructuring, phase transitions and kinetic limitations, *Atmos. Chem. Phys.*, 9, 9491–9522, doi:10.5194/acp-9-9491-2009, 2009.
- 30 Müller, L., Reinnig, M.-C., Warnke, J., and Hoffmann, Th.: Unambiguous identification of esters as oligomers in secondary organic aerosol formed from cyclohexene and cyclohexene/ $\alpha$ -pinene ozonolysis, *Atmos. Chem. Phys.*, 8, 1423–1433, doi:10.5194/acp-8-1423-2008, 2008.

**Formation,  
composition, and  
phase of  $\alpha$ -cedrene  
SOA**

Y. Zhao et al.

Title Page

Abstract

Introduction

Conclusions

References

Tables

Figures



Back

Close

Full Screen / Esc

Printer-friendly Version

Interactive Discussion



Muller, L., Reinnig, M. C., Hayen, H., and Hoffmann, T.: Characterization of oligomeric compounds in secondary organic aerosol using liquid chromatography coupled to electrospray ionization Fourier transform ion cyclotron resonance mass spectrometry, *Rapid Commun. Mass Sp.*, 23, 971–979, 2009.

5 Nah, T., Chan, M., Leone, S. R., and Wilson, K. R.: Real time in situ chemical characterization of submicrometer organic particles using direct analysis in real time-mass spectrometry, *Anal. Chem.*, 85, 2087–2095, doi:10.1021/ac302560c, 2013.

Ng, N. L., Kroll, J. H., Keywood, M. D., Bahreini, R., Varutbangkul, V., Flagan, R. C., Seinfeld, J. H., Lee, A., and Goldstein, A. H.: Contribution of first- vs. second-generation products to secondary organic aerosols formed in the oxidation of biogenic hydrocarbons, *Environ. Sci. Technol.*, 40, 2283–2297, doi:10.1021/Es052269u, 2006.

10 Pajunoja, A., Lambe, A. T., Hakala, J., Rastak, N., Cummings, M. J., Brogan, J. F., Hao, L. Q., Paramonov, M., Hong, J., Prisle, N. L., Malila, J., Romakkaniemi, S., Lehtinen, K. E. J., Laaksonen, A., Kulmala, M., Massoli, P., Onasch, T. B., Donahue, N. M., Riipinen, I., Davidovits, P., Worsnop, D. R., Petaja, T., and Virtanen, A.: Adsorptive uptake of water by semisolid secondary organic aerosols, *Geophys. Res. Lett.*, 42, 3063–3068, doi:10.1002/2015GL063142, 2015.

Pankow, J. F. and Asher, W. E.: SIMPOL.1: a simple group contribution method for predicting vapor pressures and enthalpies of vaporization of multifunctional organic compounds, *Atmos. Chem. Phys.*, 8, 2773–2796, doi:10.5194/acp-8-2773-2008, 2008.

20 Perraud, V., Bruns, E. A., Ezell, M. J., Johnson, S. N., Yu, Y., Alexander, M. L., Zelenyuk, A., Imre, D., Chang, W. L., Dabdub, D., Pankow, J. F., and Finlayson-Pitts, B. J.: Nonequilibrium atmospheric secondary organic aerosol formation and growth, *P. Natl. Acad. Sci. USA*, 109, 2836–2841, 2012.

25 Reinnig, M. C., Warnke, J., and Hoffmann, T.: Identification of organic hydroperoxides and hydroperoxy acids in secondary organic aerosol formed during the ozonolysis of different monoterpenes and sesquiterpenes by on-line analysis using atmospheric pressure chemical ionization ion trap mass spectrometry, *Rapid Commun. Mass Sp.*, 23, 1735–1741, doi:10.1002/Rcm.4065, 2009.

30 Renbaum, L. H. and Smith, G. D.: The importance of phase in the radical-initiated oxidation of model organic aerosols: reactions of solid and liquid brassidic acid particles, *Phys. Chem. Chem. Phys.*, 11, 2441–2451, doi:10.1039/b816799k, 2009.



**Formation,  
composition, and  
phase of  $\alpha$ -cedrene  
SOA**

Y. Zhao et al.

Title Page

Abstract

Introduction

Conclusions

References

Tables

Figures

◀

▶

◀

▶

Back

Close

Full Screen / Esc

Printer-friendly Version

Interactive Discussion



- Saukko, E., Lambe, A. T., Massoli, P., Koop, T., Wright, J. P., Croasdale, D. R., Pedernera, D. A., Onasch, T. B., Laaksonen, A., Davidovits, P., Worsnop, D. R., and Virtanen, A.: Humidity-dependent phase state of SOA particles from biogenic and anthropogenic precursors, *Atmos. Chem. Phys.*, 12, 7517–7529, doi:10.5194/acp-12-7517-2012, 2012.
- 5 Seinfeld, J. H. and Pandis, S. N.: *Atmospheric Chemistry and Physics: from Air Pollution to Climate Change*, 2nd edn., J. Wiley, Hoboken, N. J., USA, 2006.
- Shiraiwa, M. and Seinfeld, J. H.: Equilibration timescale of atmospheric secondary organic aerosol partitioning, *Geophys. Res. Lett.*, 39, L24801, doi:10.1029/2012GL054008, 2012.
- Shiraiwa, M., Ammann, M., Koop, T., and Poschl, U.: Gas uptake and chemical aging of semisolid organic aerosol particles, *P. Natl. Acad. Sci. USA*, 108, 11003–11008, 2011.
- 10 Shiraiwa, M., Selzle, K., and Poschl, U.: Hazardous components and health effects of atmospheric aerosol particles: reactive oxygen species, soot, polycyclic aromatic compounds and allergenic proteins, *Free Radical Res.*, 46, 927–939, doi:10.3109/10715762.2012.663084, 2012.
- 15 Slade, J. H. and Knopf, D. A.: Multiphase OH oxidation kinetics of organic aerosol: the role of particle phase state and relative humidity, *Geophys. Res. Lett.*, 41, 5297–5306, doi:10.1002/2014GL060582, 2014.
- Socrates, G.: *Infrared and Raman Characteristic Group Frequencies: Tables and Charts*, 3rd ed., Wiley, Chichester, UK, New York, USA, 2001.
- 20 Taatjes, C. A., Welz, O., Eskola, A. J., Savee, J. D., Scheer, A. M., Shallcross, D. E., Rotavera, B., Lee, E. P. F., Dyke, J. M., Mok, D. K. W., Osborn, D. L., and Percival, C. J.: Direct measurements of conformer-dependent reactivity of the Criegee intermediate  $\text{CH}_3\text{CHOO}$ , *Science*, 340, 177–180, 2013.
- Tasoglou, A. and Pandis, S. N.: Formation and chemical aging of secondary organic aerosol during the  $\beta$ -caryophyllene oxidation, *Atmos. Chem. Phys.*, 15, 6035–6046, doi:10.5194/acp-15-6035-2015, 2015.
- 25 Tolocka, M. P., Jang, M., Ginter, J. M., Cox, F. J., Kamens, R. M., and Johnston, M. V.: Formation of oligomers in secondary organic aerosol, *Environ. Sci. Technol.*, 38, 1428–1434, 2004.
- Vaden, T. D., Imre, D., Beranek, J., Shrivastava, M., and Zelenyuk, A.: Evaporation kinetics and phase of laboratory and ambient secondary organic aerosol, *P. Natl. Acad. Sci. USA*, 108, 2190–2195, 2011.
- 30







## Formation, composition, and phase of $\alpha$ -cedrene SOA

Y. Zhao et al.

Title Page

Abstract

Introduction

Conclusions

References

Tables

Figures

◀

▶

◀

▶

Back

Close

Full Screen / Esc

Printer-friendly Version

Interactive Discussion

**Table 1.** Summary of different types of flow reactor and chamber experiments.

| Exp type <sup>a</sup> | [VOC] (ppb) <sup>b</sup> | [O <sub>3</sub> ] (ppm) <sup>c</sup> | [HCOOH] or [2-EHN] | RH (%) | Reaction time | Particle size (nm) <sup>d,e</sup> | Particle mass conc. ( $\mu\text{g m}^{-3}$ ) <sup>e</sup> | Particle number conc. ( $10^6 \text{ cm}^{-3}$ ) <sup>e</sup> |
|-----------------------|--------------------------|--------------------------------------|--------------------|--------|---------------|-----------------------------------|---|---|
| <sup>2</sup> FR1      | 138                      | 14                                   | none               | < 1    | 27 s          | 15.2 ± 0.2                        | 26 ± 2  | 7.9 ± 0.2   |
| <sup>2</sup> FR2      | 138                      | 14                                   | none               | < 1    | 44 s          | 22.5 ± 0.8                        | 71 ± 8  | 7.0 ± 0.2   |
| <sup>2</sup> FR3      | 63                       | 16                                   | none               | < 1    | 30 s          | 13.1 ± 0.4                        | 10 ± 1  | 5.3 ± 0.3   |
| <sup>5</sup> FR4      | 138                      | 16                                   | none               | < 1    | 30 s          | 17.6 ± 0.9                        | 52 ± 3  | 9.4 ± 0.3   |
| <sup>2</sup> FR5      | 275                      | 16                                   | none               | < 1    | 30 s          | 25.7 ± 1.1                        | 180 ± 16  | 11.8 ± 0.6  |
| <sup>2</sup> FR6      | 138                      | 16                                   | none               | 75     | 30 s          | 16.1 ± 0.9                        | 36 ± 10   | 9.3 ± 1.7   |
| <sup>2</sup> FR7      | 138                      | 16                                   | 2 ppm HCOOH        | < 1    | 30 s          | 22.1 ± 0.4                        | 41 ± 2  | 2.7 ± 0.1   |
| <sup>2</sup> FR8      | 138                      | 16                                   | 15 ppm HCOOH       | < 1    | 30 s          | 22.0 ± 0.8                        | 25 ± 1  | 1.5 ± 0.1   |
| <sup>4</sup> CH1      | 34                       | 1.5                                  | none               | < 1    | 30 min        | 66 ± 2                            | 73 ± 6  | 0.34 ± 0.02   |
| <sup>4</sup> CH2      | 34                       | 1.5                                  | none               | 72     | 30 min        | 64 ± 2                            | 66 ± 4  | 0.34 ± 0.03   |
| <sup>3</sup> CH3      | 1000                     | 0.12                                 | none               | < 1    | 30 min        | 111 ± 1                           | 363 ± 37  | 0.37 ± 0.03   |
| <sup>3</sup> CH4      | 215                      | 1.5                                  | none               | < 1    | 60 min        | 140 ± 3                           | 984 ± 186   | 0.40 ± 0.02   |
| <sup>2</sup> CH5      | 215                      | 1.5                                  | 400 ppb 2-EHN      | < 1    | 60 min        | 127 ± 5                           | 663 ± 44  | 0.35 ± 0.02   |

<sup>a</sup> FR and CH represent flow reactor and chamber experiments, respectively. The numbers in front of the labels represent the times an experiment was repeated.

<sup>b</sup> The concentrations were calculated from the amount of  $\alpha$ -cedrene liquid injected into the flow reactor and chamber, and the total gas flow.

<sup>c</sup> High O<sub>3</sub> concentration is needed to get enough reaction to form particles in less than a min in FR experiments.

<sup>d</sup> Geometric mean diameter; the size distributions of SOA formed in the flow reactor are given in Figs. S1 and 11.

<sup>e</sup> All the data are given as "average value ± one standard deviation". SOA mass concentrations are obtained using a particle density of  $1.1 \text{ g cm}^{-3}$  (Yao et al., 2014). The chamber SOA data are given for 30 or 60 min reaction times, and were not corrected for the wall loss.



## Formation, composition, and phase of $\alpha$ -cedrene SOA

Y. Zhao et al.

**Table 2.** Accurate mass and elemental formulae for P1 and P2 products formed from  $\alpha$ -cedrene ozonolysis measured by ESI-ToF-MS.

| Products <sup>a</sup> | ESI+ mode ([M + Na] <sup>+</sup> ) |   |                            |                           |                           | ESI- mode ([M - H] <sup>-</sup> ) |  |                            |                           |                           |
|-----------------------|------------------------------------|---|----------------------------|---------------------------|---------------------------|-----------------------------------|--|----------------------------|---------------------------|---------------------------|
|                       | Observed accurate mass (Da)        | Elemental formula                                 | Calculated exact mass (Da) | Absolute mass error (mDa) | Relative mass error (ppm) | Observed accurate mass (Da)       | Elemental formula                              | Calculated exact mass (Da) | Absolute mass error (mDa) | Relative mass error (ppm) |
| P1-245                | 245.1525                           | C <sub>14</sub> H <sub>22</sub> O <sub>2</sub> Na | 245.1517                   | 0.8                       | 3.3                       | – <sup>b</sup>                    |  |                            |                           |                           |
| P1-247                | 247.1326                           | C <sub>13</sub> H <sub>20</sub> O <sub>3</sub> Na | 247.1310                   | 1.6                       | 6.4                       | 223.1341                          | C <sub>13</sub> H <sub>19</sub> O <sub>3</sub> | 223.1334                   | 0.7                       | 3.1                       |
| P1-259                | 259.1681                           | C <sub>15</sub> H <sub>24</sub> O <sub>2</sub> Na | 259.1674                   | 0.7                       | 2.7                       | – <sup>b</sup>                    |  |                            |                           |                           |
| P1-261                | – <sup>b</sup>                     |   |                            |                           |                           | 237.1494                          | C <sub>14</sub> H <sub>21</sub> O <sub>3</sub> | 237.1491                   | 0.3                       | 1.3                       |
| P1-275                | 275.1628                           | C <sub>15</sub> H <sub>24</sub> O <sub>3</sub> Na | 275.1623                   | 0.5                       | 1.8                       | 251.1646                          | C <sub>15</sub> H <sub>23</sub> O <sub>3</sub> | 251.1647                   | –0.1                      | –0.4                      |
| P1-277                | 277.1422                           | C <sub>14</sub> H <sub>22</sub> O <sub>4</sub> Na | 277.1416                   | 0.6                       | 2.2                       | 253.1447                          | C <sub>14</sub> H <sub>21</sub> O <sub>4</sub> | 253.1440                   | 0.7                       | 2.8                       |
| P1-289                | 289.1431                           | C <sub>15</sub> H <sub>22</sub> O <sub>4</sub> Na | 289.1416                   | 1.5                       | 5.2                       | 265.1476                          | C <sub>15</sub> H <sub>21</sub> O <sub>4</sub> | 265.1440                   | 3.6                       | 13.6 <sup>d</sup>         |
| P1-291                | 291.1577                           | C <sub>15</sub> H <sub>24</sub> O <sub>4</sub> Na | 291.1572                   | 0.5                       | 1.6                       | 267.1607                          | C <sub>15</sub> H <sub>23</sub> O <sub>4</sub> | 267.1596                   | 1.1                       | 4.1                       |
| P1-305                | 305.1370                           | C <sub>15</sub> H <sub>22</sub> O <sub>5</sub> Na | 305.1365                   | 0.5                       | 1.7                       | – <sup>b</sup>                    |  |                            |                           |                           |
| P1-307                | 307.1516                           | C <sub>15</sub> H <sub>24</sub> O <sub>5</sub> Na | 307.1521                   | –0.5                      | –1.8                      | 283.1554                          | C <sub>15</sub> H <sub>23</sub> O <sub>5</sub> | 283.1545                   | 0.9                       | 3.2                       |
| P1-321                | 321.1308                           | C <sub>15</sub> H <sub>22</sub> O <sub>6</sub> Na | 321.1314                   | –0.6                      | –1.9                      | 297.1345                          | C <sub>15</sub> H <sub>21</sub> O <sub>6</sub> | 297.1338                   | 0.7                       | 2.4                       |
| P1-323                | 323.1465                           | C <sub>15</sub> H <sub>24</sub> O <sub>6</sub> Na | 323.1471                   | –0.6                      | –1.9                      | 299.1492                          | C <sub>15</sub> H <sub>23</sub> O <sub>6</sub> | 299.1495                   | –0.3                      | –1.0                      |
| P2-481                | 481.3298                           | C <sub>29</sub> H <sub>46</sub> O <sub>4</sub> Na | 481.3294                   | 0.4                       | 0.8                       | – <sup>b</sup>                    |  |                            |                           |                           |
| P2-497                | 497.3262                           | C <sub>29</sub> H <sub>46</sub> O <sub>5</sub> Na | 497.3243                   | 1.9                       | 3.8                       | 473.3271                          | C <sub>29</sub> H <sub>45</sub> O <sub>5</sub> | 473.3267                   | 0.4                       | 0.9                       |
| P2-511 <sup>c</sup>   | 511.3337                           | C <sub>30</sub> H <sub>48</sub> O <sub>5</sub> Na | 511.3399                   | –6.2                      | –12.1 <sup>d</sup>        | 487.3086                          | C <sub>29</sub> H <sub>43</sub> O <sub>6</sub> | 487.3060                   | 2.6                       | 5.3                       |
| P2-513                | 513.3203                           | C <sub>29</sub> H <sub>46</sub> O <sub>6</sub> Na | 513.3192                   | 1.1                       | 2.1                       | 489.3215                          | C <sub>29</sub> H <sub>45</sub> O <sub>6</sub> | 489.3216                   | –0.1                      | –0.2                      |
| P2-527                | 527.3317                           | C <sub>30</sub> H <sub>48</sub> O <sub>6</sub> Na | 527.3348                   | –3.1                      | –5.8                      | 503.3387                          | C <sub>30</sub> H <sub>47</sub> O <sub>6</sub> | 503.3372                   | 1.5                       | 3.0                       |
| P2-543                | 543.3309                           | C <sub>30</sub> H <sub>48</sub> O <sub>7</sub> Na | 543.3298                   | 1.1                       | 2.0                       | 519.3320                          | C <sub>30</sub> H <sub>47</sub> O <sub>7</sub> | 519.3322                   | –0.2                      | –0.4                      |

<sup>a</sup> Labels "P1-xxx" and "P2-xxx" denote P1 and P2 products having a nominal mass of xxx for their sodiated ions, respectively.

<sup>b</sup> Accurate mass was not measured because of the very low ion intensity or the strong interference from other ions such as impurities.

<sup>c</sup> Different formulas for P2-511 were identified in ESI+ and ESI- modes, which correspond, respectively, to aldol condensation products (P2-511-3 and P2-511-4) and esters (P2-511-1 and P2-511-2) as shown in Fig. 10c.

<sup>d</sup> The relatively large mass errors likely result from unknown interferences for P1-289 in ESI- mode and P2-511 in ESI+ mode. The given formulas are the closest to the observed masses but may not be correct because of the interferences.

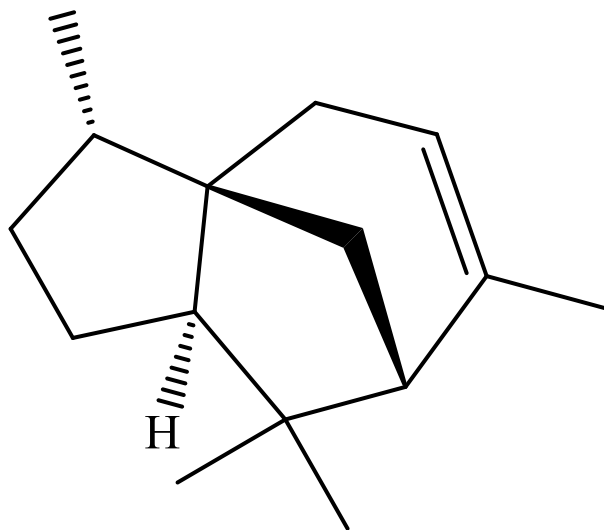


**Figure 1.** The structure of  $\alpha$ -cedrene.

**Formation,  
composition, and  
phase of  $\alpha$ -cedrene  
SOA**

Y. Zhao et al.

Title Page

Abstract

Introduction

Conclusions

References

Tables

Figures



Back

Close

Full Screen / Esc

Printer-friendly Version

Interactive Discussion



## Formation, composition, and phase of $\alpha$ -cedrene SOA

Y. Zhao et al.

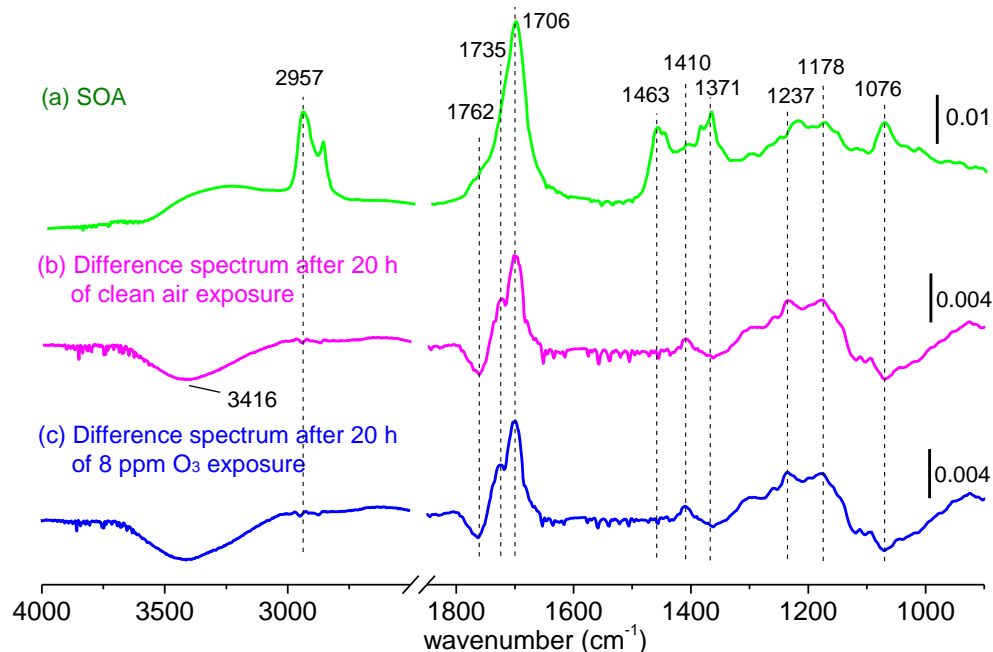


**Figure 2.** (a) A typical ATR-FTIR spectrum of SOA from ozonolysis of  $\alpha$ -cedrene in the chamber (experiment CH4, Table 1). This spectrum is obtained from  $\log_{10}(S_0/S_1)$  where  $S_0$  and  $S_1$  are the single beam spectra of the clean crystal and SOA covered crystal recorded immediately following impaction. (b) and (c) typical difference spectra of SOA after 20 h of exposure to a flow of clean and 8 ppm  $\text{O}_3$ -containing dry air. These spectra are  $\log_{10}(S_1/S_{20})$  where  $S_1$  is the single beam spectrum of SOA covered crystal collected immediately following impaction and  $S_{20}$  is that after 20 h of air or  $\text{O}_3$  exposure. The positive and negative peaks in the difference spectra represent an increase and decrease, respectively, of the functional groups in SOA over 20 h of exposure.

## Formation, composition, and phase of $\alpha$ -cedrene SOA

Y. Zhao et al.

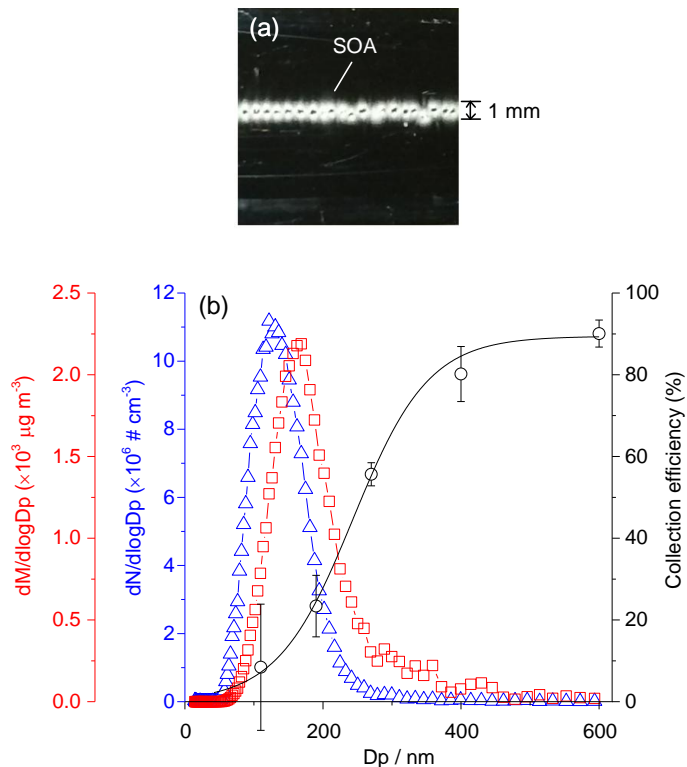


**Figure 3.** (a) Digital photograph of a typical impaction pattern of SOA formed by ozonolysis of  $\alpha$ -cedrene in the presence of 2-EHN in the chamber (experiment CH5, Table 1). The photograph shows a 1 cm  $\times$  1 cm section of the crystal. The impacted SOA forms a narrow film  $\sim$  1 mm in width along the centerline of the crystal. (b) The number (blue triangles) and mass (red squares) weighted size distribution of chamber  $\alpha$ -cedrene SOA formed in the presence of 2-EHN. Also shown is the collection efficiency of the impactor as a function of particle diameter (black circle) measured using carboxylate-modified latex (CML) spheres in a previous study (Kidd et al., 2014b).

Formation,  
composition, and  
phase of  $\alpha$ -cedrene  
SOA

Y. Zhao et al.

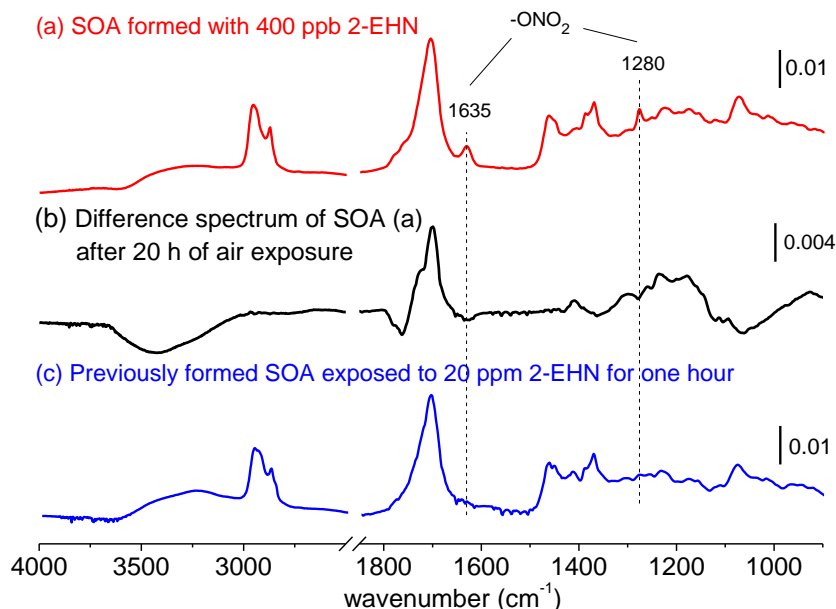


**Figure 4.** (a) A typical ATR-FTIR spectrum of SOA from ozonolysis of  $\alpha$ -cedrene in the presence of gas phase 2-EHN in the chamber (experiment CH5, Table 1). This spectrum is obtained from  $\log_{10}(S_0/S_1)$  where  $S_0$  and  $S_1$  are the single beam spectra of the clean crystal and SOA covered crystal recorded immediately following impaction. (b) A typical difference spectrum of SOA after 20 h of exposure to a flow of clean dry air. This spectrum is  $\log_{10}(S_1/S_{20})$  where  $S_1$  and  $S_{20}$  are the single beam spectra of SOA covered crystal recorded immediately following impaction and after 20 h of air exposure. The positive and negative peaks in the spectra represent an increase and decrease in the functional groups over 20 h of air exposure, respectively. (c) ATR-FTIR spectrum of SOA formed without 2-EHN following exposure to a flow of dry air containing 20 ppm 2-EHN for one hour. This spectrum is derived from  $\log_{10}(S_0/S_1)$  where  $S_0$  and  $S_1$  are the single beam spectra of the clean crystal and SOA covered crystal exposed to 20 ppm 2-EHN for one hour, respectively.

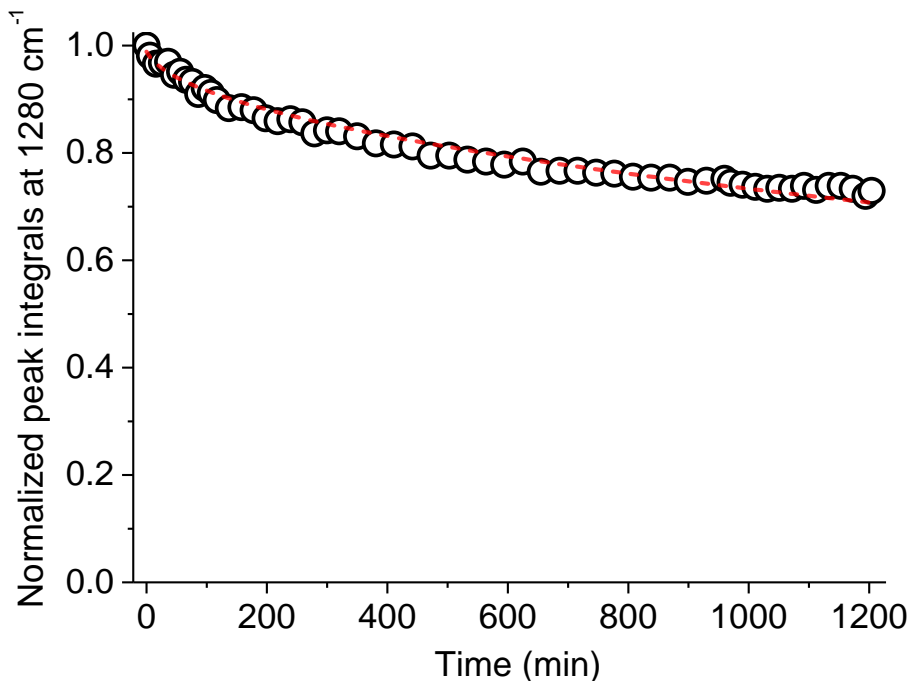


**Figure 5.** The normalized integrated area of  $-\text{ONO}_2$  peak at  $1280\text{ cm}^{-1}$  as a function of time over 20 h of clean, dry air exposure. The red dash line is a best fit of the evaporation data to Eq. (1).

**Formation,  
composition, and  
phase of  $\alpha$ -cedrene  
SOA**

Y. Zhao et al.

Title Page

Abstract

Introduction

Conclusions

References

Tables

Figures

◀

▶

◀

▶

Back

Close

Full Screen / Esc

Printer-friendly Version

Interactive Discussion



## Formation, composition, and phase of $\alpha$ -cedrene SOA

Y. Zhao et al.

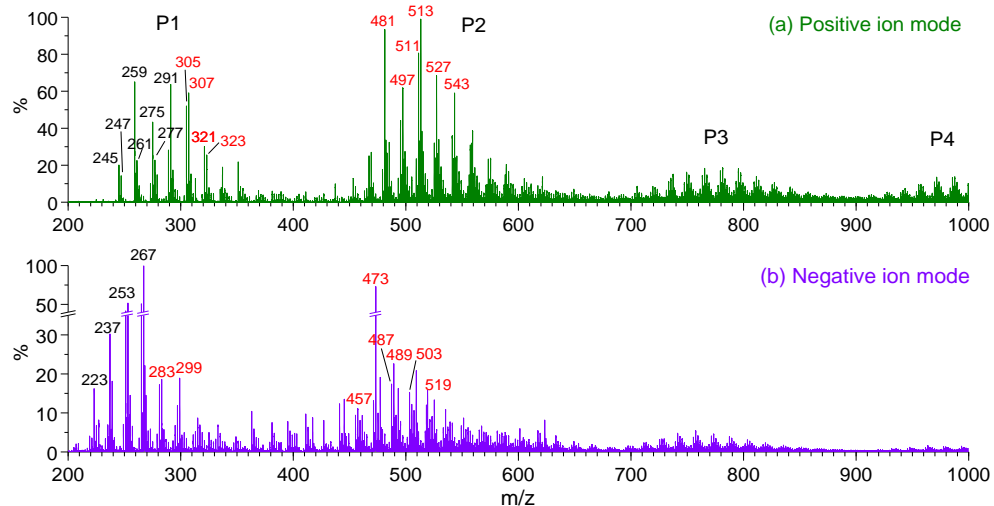


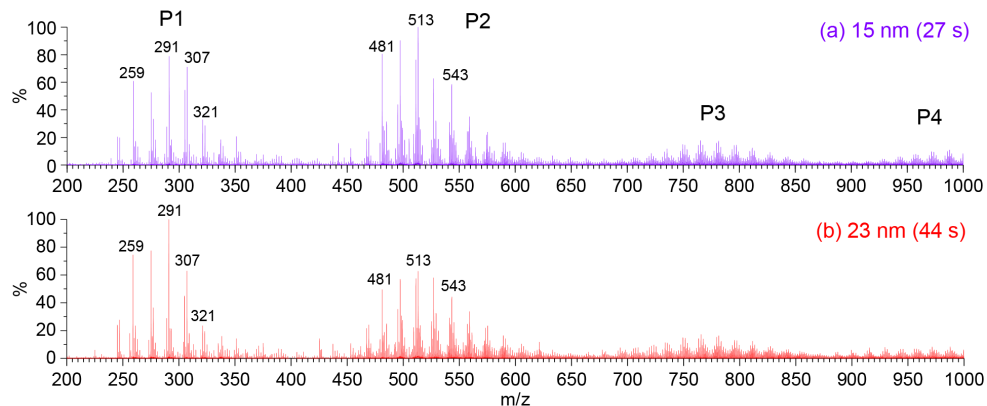
**Figure 6.** ESI mass spectra of SOA formed from ozonolysis of  $\alpha$ -cedrene in the flow reactor (experiment FR4, Table 1) in **(a)** positive and **(b)** negative ion modes. Black and red labels indicate the previously reported (Jaoui et al., 2004, 2013; Reinnig et al., 2009; Yao et al., 2014) and newly observed products, respectively. P1 represents the low molecular weight products, and P2, P3, and P4 denote higher molecular weight products formed by combinations of two, three, or four of the P1 products, respectively.

[Title Page](#)[Abstract](#)[Introduction](#)[Conclusions](#)[References](#)[Tables](#)[Figures](#)[◀](#)[▶](#)[◀](#)[▶](#)[Back](#)[Close](#)[Full Screen / Esc](#)[Printer-friendly Version](#)[Interactive Discussion](#)



## Formation, composition, and phase of $\alpha$ -cedrene SOA

Y. Zhao et al.

[Title Page](#)[Abstract](#)[Introduction](#)[Conclusions](#)[References](#)[Tables](#)[Figures](#)[◀](#)[▶](#)[◀](#)[▶](#)[Back](#)[Close](#)[Full Screen / Esc](#)[Printer-friendly Version](#)[Interactive Discussion](#)

**Figure 7.** ESI(+) mass spectra of polydisperse SOA with geometric mean diameter of (a) 15 nm and (b) 23 nm formed from ozonolysis of  $\alpha$ -cedrene in the flow reactor at 27 and 44 s reaction times, respectively, under dry conditions (experiments FR1 and FR2, Table 1). The size distributions of SOA are shown in Fig. S1a. Note that these experiments were conducted as a separate series from other experiments. Because ESI-MS sensitivity changes over long periods (a month or more), the intensity ratios of oligomer to P1 products in the mass spectra shown here cannot be directly compared with other mass spectra obtained in this work. However, those ratios in the above mass spectra are comparable with each other as they were acquired on the timescale of days, over which ESI-MS sensitivity is essentially constant.

**Formation,  
composition, and  
phase of  $\alpha$ -cedrene  
SOA**

Y. Zhao et al.

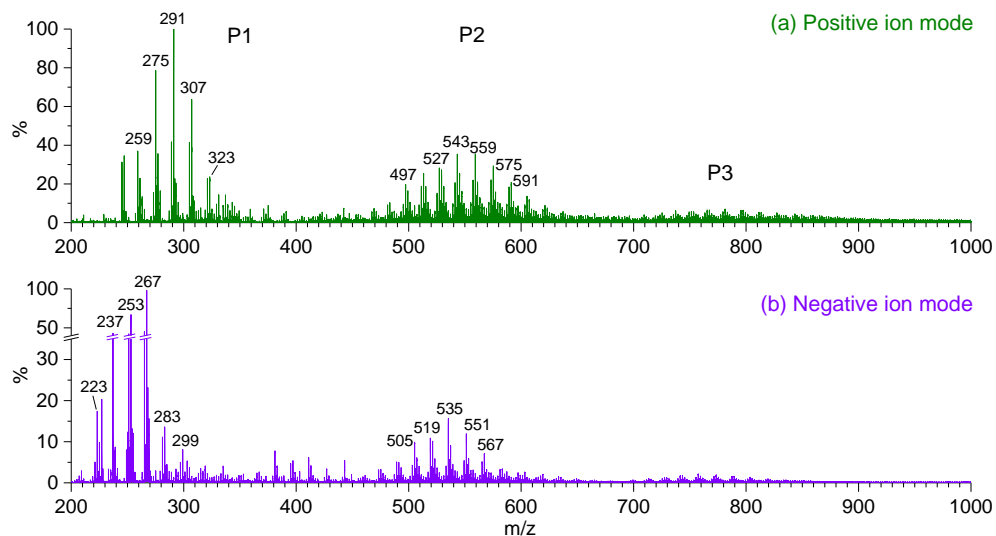


**Figure 8.** ESI mass spectra of SOA formed from ozonolysis of  $\alpha$ -cedrene in the chamber (experiment CH1, Table 1) in **(a)** positive and **(b)** negative ion modes.

[Title Page](#)[Abstract](#)[Introduction](#)[Conclusions](#)[References](#)[Tables](#)[Figures](#)[◀](#)[▶](#)[◀](#)[▶](#)[Back](#)[Close](#)[Full Screen / Esc](#)[Printer-friendly Version](#)[Interactive Discussion](#)



## Formation, composition, and phase of $\alpha$ -cedrene SOA

Y. Zhao et al.

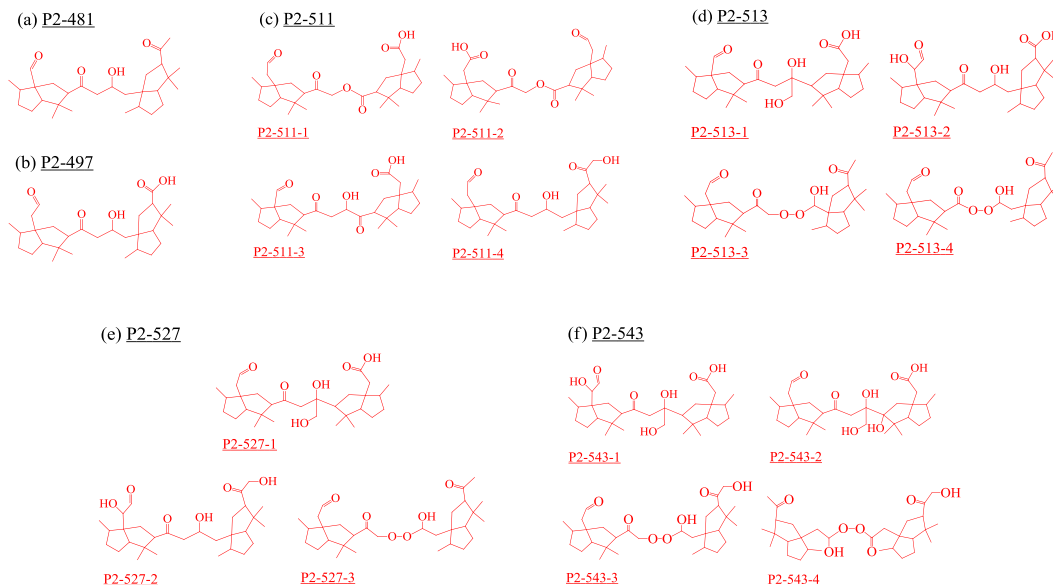


**Figure 10.** The potential structures for the P2 products corresponding to the  $[M+Na]^+$  ions of **(a)**  $m/z$  481, **(b)**  $m/z$  497, **(c)**  $m/z$  511, **(d)**  $m/z$  513, **(e)**  $m/z$  527, and **(f)**  $m/z$  543 formed from  $\alpha$ -cedrene ozonolysis. Label “P2-xxx” represents a P2 product, the sodiated ion of which has a nominal mass of xxx. Label “P2-xxx- $n$ ” ( $n = 1-4$ ) indicates different potential structures for the product “P2-xxx”.

Title Page

Abstract

Introduction

Conclusions

References

Tables

Figures



Back

Close

Full Screen / Esc

Printer-friendly Version

Interactive Discussion



**Formation,  
composition, and  
phase of  $\alpha$ -cedrene  
SOA**

Y. Zhao et al.

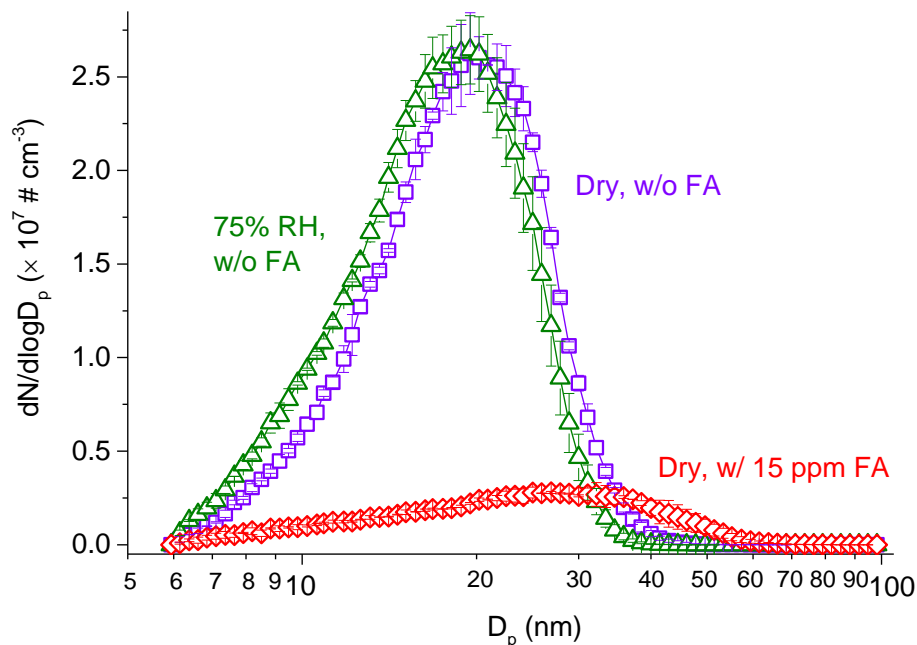


**Figure 11.** The size distributions of SOA formed from ozonolysis of  $\alpha$ -cedrene in the flow reactor under dry conditions (purple squares, experiment FR4), at 75% RH (green triangles, experiment FR6), or in the presence of 15 ppm formic acid (red diamonds, experiment FR8).

[Title Page](#)[Abstract](#)[Introduction](#)[Conclusions](#)[References](#)[Tables](#)[Figures](#)[◀](#)[▶](#)[◀](#)[▶](#)[Back](#)[Close](#)[Full Screen / Esc](#)[Printer-friendly Version](#)[Interactive Discussion](#)

Formation,  
composition, and  
phase of  $\alpha$ -cedrene  
SOA

Y. Zhao et al.

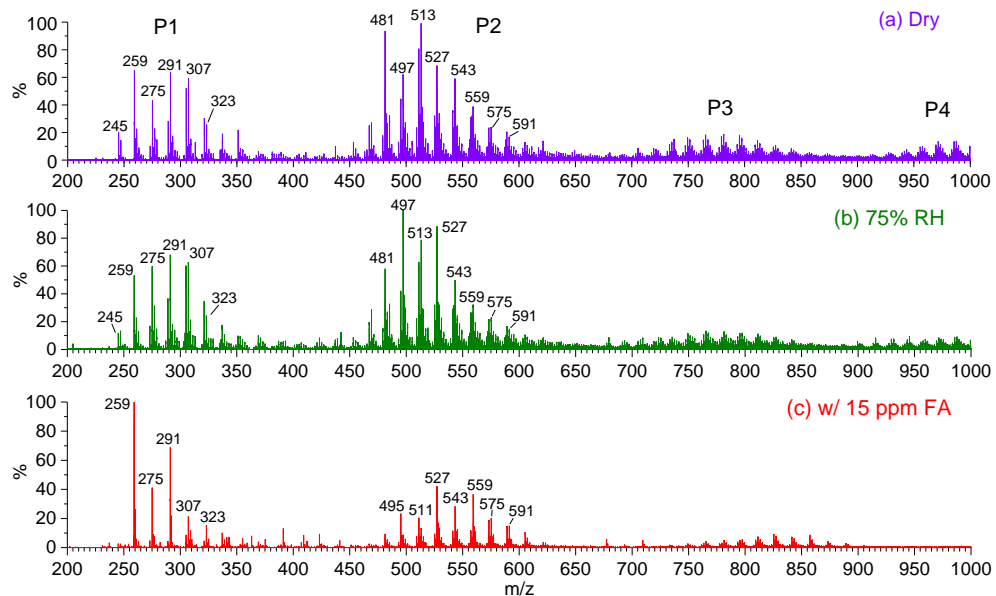


**Figure 12.** ESI(+)-mass spectra of polydisperse SOA formed from ozonolysis of  $\alpha$ -cedrene in the flow reactor **(a)** under dry conditions (experiment FR4), **(b)** at 75 % RH (experiment FR6), and **(c)** with 15 ppm formic acid (experiment FR8).

[Title Page](#)[Abstract](#)[Introduction](#)[Conclusions](#)[References](#)[Tables](#)[Figures](#)[◀](#)[▶](#)[◀](#)[▶](#)[Back](#)[Close](#)[Full Screen / Esc](#)[Printer-friendly Version](#)[Interactive Discussion](#)

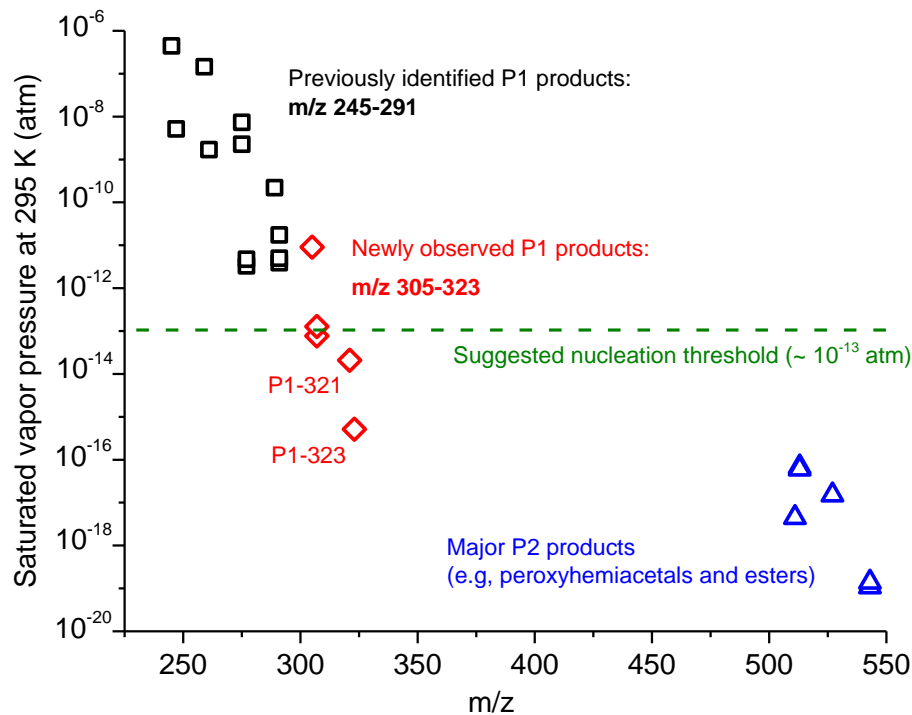


**Figure 13.** Saturated vapor pressures of typical P1 and P2 products in  $\alpha$ -cedrene SOA estimated by taking the average of the predictions from SIMPOL.1 and EVAPORATION. The dashed line indicates the upper limit of saturated organic vapor pressure for nucleation.